PLOS BIOLOGY

DISCOVERY REPORT

Stress-dependent cell stiffening by tardigrade tolerance proteins that reversibly form a filamentous network and gel

Akihiro Tanaka[1], Tomomi Nakano[1], Kento Watanabe[1], Kazutoshi Masuda[2,3], Gen Honda[2,3], Shuichi Kamata[1], Reitaro Yasui[1], Hiroko Kozuka-Hata[4], Chiho Watanabe[2,3¤], Takumi Chinen[5], Daiju Kitagawa[5], Satoshi Sawai[1,3], Masaaki Oyama[4], Miho Yanagisawa[2,3], Takekazu Kunieda[1]*

1 Department of Biological Sciences, Graduate School of Science, The University of Tokyo, Bunkyo-ku, Tokyo, Japan, **2** Komaba Institute for Science, Graduate School of Arts and Sciences, The University of Tokyo, Meguro-ku, Tokyo, Japan, **3** Department of Basic Science, Graduate School of Arts and Sciences, The University of Tokyo, Meguro-ku, Tokyo, Japan, **4** Medical Proteomics Laboratory, The Institute of Medical Science, The University of Tokyo, Minato-ku, Tokyo, Japan, **5** Department of Physiological Chemistry, Graduate School of Pharmaceutical Sciences, The University of Tokyo, Bunkyo-ku, Tokyo, Japan

¤ Current address: Graduate School of Integrated Sciences for Life, School of Integrated Arts and Sciences, Hiroshima University, Higashi-Hiroshima, Hiroshima, Japan
* kunieda@bs.s.u-tokyo.ac.jp

OPEN ACCESS

Citation: Tanaka A, Nakano T, Watanabe K, Masuda K, Honda G, Kamata S, et al. (2022) Stress-dependent cell stiffening by tardigrade tolerance proteins that reversibly form a filamentous network and gel. PLoS Biol 20(9): e3001780. https://doi.org/10.1371/journal.pbio.3001780

Academic Editor: Carole A. Parent, University of Michigan, UNITED STATES

Received: September 19, 2021

Accepted: August 2, 2022

Published: September 6, 2022

Peer Review History: PLOS recognizes the benefits of transparency in the peer review process; therefore, we enable the publication of all of the content of peer review and author responses alongside final, published articles. The editorial history of this article is available here: https://doi.org/10.1371/journal.pbio.3001780

Abstract

Tardigrades are able to tolerate almost complete dehydration by entering a reversible ametabolic state called anhydrobiosis and resume their animation upon rehydration. Dehydrated tardigrades are exceptionally stable and withstand various physical extremes. Although trehalose and late embryogenesis abundant (LEA) proteins have been extensively studied as potent protectants against dehydration in other anhydrobiotic organisms, tardigrades produce high amounts of tardigrade-unique protective proteins. Cytoplasmic-abundant heat-soluble (CAHS) proteins are uniquely invented in the lineage of eutardigrades, a major class of the phylum Tardigrada and are essential for their anhydrobiotic survival. However, the precise mechanisms of their action in this protective role are not fully understood. In the present study, we first postulated the presence of tolerance proteins that form protective condensates via phase separation in a stress-dependent manner and searched for tardigrade proteins that reversibly form condensates upon dehydration-like stress. Through a comprehensive search using a desolvating agent, trifluoroethanol (TFE), we identified 336 proteins, collectively dubbed "TFE-Dependent ReversiblY condensing Proteins (T-DRYPs)." Unexpectedly, we rediscovered CAHS proteins as highly enriched in T-DRYPs, 3 of which were major components of T-DRYPs. We revealed that these CAHS proteins reversibly polymerize into many cytoskeleton-like filaments depending on hyperosmotic stress in cultured cells and undergo reversible gel-transition in vitro. Furthermore, CAHS proteins increased cell stiffness in a hyperosmotic stress-dependent manner and counteract the cell shrinkage caused by osmotic pressure, and even improved the survival against hyperosmotic stress. The conserved putative helical C-terminal region is necessary and sufficient for filament formation by CAHS proteins, and mutations disrupting the secondary structure of this region impaired both the filament formation and the gel transition. On the

Data Availability Statement: All mass spectrometry proteomics data are available from the jPOST repository of ProteomeXchange Consortium (dataset identifier PXD030241). All other relevant data are within the paper and its Supporting Information files.

Funding: This work was supported by Japan Society for the Promotion of Science (JSPS; https://www.jsps.go.jp/english/) KAKENHI Grant Numbers JP16H01632, JP16H02951, JP18H04969, JP20H04332, JP20K20580, JP21H05279 (to TK); JP21J11385 (to AT); and JP21H05871 (to MY). MY received the funding from KOSE Cosmetology Research Foundation. The funders had no role in study design, data collection and analysis, decision to publish, or preparation of the manuscript.

Competing interests: The authors have declared that no competing interests exist.

Abbreviations: AFM, atomic force microscope; CAHS, cytoplasmic-abundant heat-soluble; CD, circular dichroism; DSC, differential scanning calorimetry; FRAP, fluorescence recovery after photobleaching; HBSS, Hanks' Balanced Salt Solution; IF, intermediate filament; LEA, late embryogenesis abundant; PI, propidium iodide; T-DRYP, TFE-dependent reversibly condensing protein; TFE, trifluoroethanol.

basis of these results, we propose that CAHS proteins are novel cytoskeleton-like proteins that form filamentous networks and undergo gel-transition in a stress-dependent manner to provide on-demand physical stabilization of cell integrity against deformative forces during dehydration and could contribute to the exceptional physical stability in a dehydrated state.

Introduction

Water is an essential molecule for maintaining the metabolic activity and cellular integrity of living organisms. Some organisms, however, can tolerate almost complete dehydration by entering a reversible ametabolic state called anhydrobiosis [1]. Tardigrades, also known as water bears, are a prominent example of such desiccation-tolerant animals [2]. Under a drying environment, tardigrades gradually lose almost all body water and concurrently contract their bodies to a shrunken round form called a tun. Dehydrated tardigrades are exceptionally stable and can withstand various physically extreme environments including exposure to space [3,4]. Even after exposure to extreme stressors, tardigrades can reanimate within a few dozen minutes after rehydration.

Several tolerance molecules against dehydration stress have been identified in various organisms. One of the most analyzed molecules is the nonreducing disaccharide, trehalose. A significant amount of trehalose accumulates during desiccation in several anhydrobiotic animals, such as sleeping chironomids [5], brine shrimp [6], and some nematodes [7], some of which require trehalose synthesis for anhydrobiotic survival [8]. Trehalose is proposed to play its protective roles through 2 modes of action: water replacement, in which trehalose substitutes for water molecules, and vitrification, in which trehalose preserves cell components in an amorphous solid (glassy) state [9]. In tardigrades, however, no or only a little amount of trehalose accumulates, even in dehydrated states of the anhydrobiotic species [10], and a recent study suggested that trehalose synthesis genes in tardigrades are acquired in only limited lineages via horizontal transfer after the establishment of the anhydrobiotic ability in ancestral eutardigrades [11], suggesting the presence of a trehalose-independent anhydrobiosis mechanism in tardigrades.

Late embryogenesis abundant (LEA) proteins are another example of tolerance molecules. LEA proteins are principally unstructured proteins originally identified in desiccating plant seeds and later found in several anhydrobiotic animals [12]. LEA proteins have many proposed roles, including stabilization of vitrified trehalose, molecular shielding of client biomolecules, and sequestration of ions [12]. LEA proteins can suppress dehydration-dependent denaturation of enzymes and have strong synergistic protective effects with trehalose [13]. The LEA proteins of brine shrimp were recently reported to undergo phase separation to form droplet condensates upon dehydration and to increase the desiccation tolerance of insect cells [14].

Through a search for LEA-like heat-soluble proteins that remain soluble even after boiling in tardigrades, we previously identified cytoplasmic-abundant heat-soluble (CAHS) proteins from one of the toughest tardigrade species, *Ramazzottius varieornatus* [15]. CAHS proteins exhibited almost no similarity with non-tardigrade proteins, and later genome and transcriptome analyses suggested that CAHS proteins are present only in eutardigrades, one of the major classes of the phylum Tardigrada [11,16–20]. Despite the absence of sequence similarity between CAHS proteins and LEA proteins, they share similar biochemical properties, e.g., high-hydrophilicity supporting heat-solubility and structural transition from the disordered state in hydration to a helix under desolvating or dehydrated conditions [12,15]. Like LEA

proteins, CAHS proteins can protect enzymes from dehydration stress [18] and *R. varieornatus* produces a remarkable amount of CAHS proteins rather than trehalose and LEA proteins. Knockdown of several CAHS genes that impaired the anhydrobiotic survival revealed that CAHS proteins are involved in the desiccation tolerance of eutardigrades [18]. Although CAHS proteins were proposed to act as a vitrifying agent based on a shift in differential scanning calorimetry (DSC), this hypothesis was recently counter-argued as such a shift could be explained by the evaporation of residual water [21], and the molecular mechanism remains to be elucidated.

Dehydration stress leads to the cell shrinkage, causing severe deformative mechanical stress affecting the integrity of cell structures. To counteract the deformative forces, cytoskeletons like intermediate filaments (IFs) are generally principal players in ordinary animal cells [22,23]. Interestingly, canonical cytoplasmic IFs are missing in Panarthropoda including tardigrades and arthropods. Tardigrades have a tardigrade-unique IF protein called cytotardin, which is not homologous to any cytoplasmic IFs in other animals and rather derives from the nuclear filament protein lamin [24]. Cytotardin does not localize to the nucleus because it lacks a nuclear localization signal and instead forms belt-like filaments beneath the plasma membrane encircling epithelial cells, suggesting its contribution to the mechanical strengthening of epithelial tissues. In tardigrades, no IFs are known to form scaffold-like filamentous networks in the cytosol, which is thought to effectively counteract the deformative forces in many other animal cells [25,26].

In this study, we postulated the presence of tolerance proteins that form protective condensates in a stress-dependent manner and searched for such proteins in tardigrade lysate using a desolvating agent, trifluoroethanol (TFE). Among more than 300 identified proteins that we collectively dubbed "TFE-dependent reversibly condensing proteins (T-DRYPs)," we unexpectedly rediscovered CAHS proteins as highly enriched and major components of T-DRYPs. Further analyses revealed that in response to stress, CAHS reversibly forms many cytoskeleton-like filaments in cultured cells and also exhibits reversible gelation in vitro. CAHS proteins increase the mechanical strength of cultured cells and improve their resistance to dehydration-like stress. We also examined the structural basis required for filament formation by deletion and point mutation analyses. By studying the generated filament-impaired mutants, we confirmed that the filament-forming ability is the basis for the gel transition of CAHS proteins. On the basis of these results, we propose a new tolerance model in which CAHS proteins act as a kind of cytoskeleton that reversibly forms intracellular filamentous networks in response to dehydration and induces gel transition that increases mechanical strength of cells and contributes to the desiccation tolerance of tardigrades.

Results

Trifluoroethanol-dependent reversibly condensing proteins (T-DRYPs) are identified from *Ramazzottius varieornatus*

We designed the experimental scheme shown in Fig 1A to identify tardigrade proteins that form condensates in response to dehydration-like stress in a reversible manner. We began with the lysate of the desiccation-tolerant tardigrade species *R. varieornatus*, because this species constitutively expresses the tolerance proteins and its genome sequence is available [16]. First, we added a desolvating agent, TFE to a soluble fraction of *R. varieornatus* lysate to induce condensation in a dehydration-like state. TFE is a cosolvent that affects the protein conformation by displacing water molecules from the surface of polypeptides [27] and/or destabilizing an aqueous solvation of polypeptide backbone [28], which indirectly promotes intramolecular hydrogen bonding and stabilizes the secondary structures of proteins. TFE is also known to

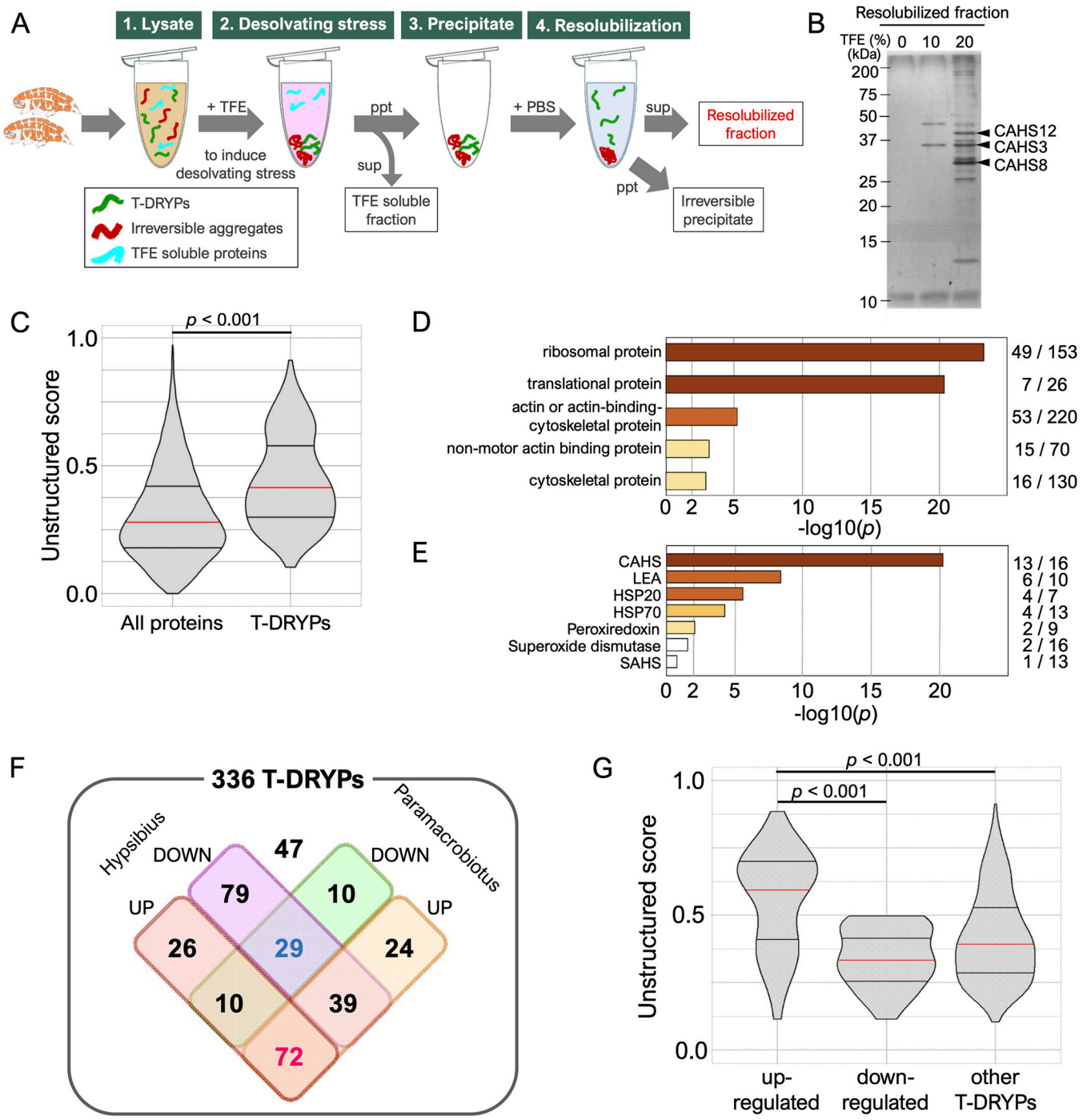

Fig 1. Isolation and characterization of T-DRYPs. (A) Experimental scheme of T-DRYP isolation from tardigrade lysate. (B) SDS-PAGE image of the resolubilized fractions with 0%, 10%, or 20% TFE treatment. (C) Comparison of the unstructured score distributions between all tardigrade proteins and T-DRYPs. (D) Enrichment analysis of the PANTHER protein class in T-DRYPs. Ribosomal proteins and cytoskeletal proteins were significantly enriched. The numbers of the corresponding proteins detected in T-DRYPs and all tardigrade proteomes are shown on the right, respectively. (E) Enrichment analysis of stress-related proteins in T-DRYPs. CAHS proteins were significantly enriched in T-DRYPs. (F) Venn diagram of T-DRYPs classified by up- or down-regulation upon desiccation in orthologs of 2 other tardigrade species. (G) Comparison of unstructured score distributions among the differently regulated protein groups in T-DRYPs. "Up-regulated" and "down-regulated" indicate up-regulated or down-regulated proteins in both species, respectively. Proteins up-regulated upon desiccation exhibited higher unstructured scores. Red and 2 black horizontal bars in violin plot indicate the 50th, 25th, and 75th percentiles, respectively. Statistical analyses were performed with the Wilcoxon rank sum test in (C) and the Steel–Dwass test in (G). The underlying numerical data are available in S4 Data (C, D, and G) in S2 Data (E) and in S1 Data (F). CAHS, cytoplasmic-abundant heat-soluble; T-DRYP, TFE-dependent reversibly condensing protein; TFE, trifluoroethanol.

https://doi.org/10.1371/journal.pbio.3001780.g001

promote alpha-helix formation in several desiccation-tolerance proteins, such as LEA and CAHS proteins as dehydration do [15,29,30]. The TFE-condensed proteins were collected as precipitates and resolubilized with TFE-free PBS to mimic rehydration (resolvation). Treatment with higher concentration of TFE increased the number of proteins detected in the resolubilized fraction (Figs 1B and S1). As treatment with 20% and 30% TFE had similar effects, we considered 20% TFE to be an adequate stress condition for this screening (S1 Fig). When treated with TFE at 20% or higher, many proteins, especially those with a high molecular weight, were detected in the irreversibly precipitated fraction, indicating that only the selected proteins were retrieved in the resolubilized fraction.

We identified 336 proteins in the resolubilized fraction (20% TFE) by nanoflow liquid chromatography-tandem mass spectrometry (nanoLC-MS/MS) and collectively termed these proteins "TFE-Dependent ReversiblY condensing Proteins (T-DRYPs)" (S1 Data). Because reversible condensation is a characteristic property expected for unstructured proteins, we calculated the unstructured score of each protein in T-DRYPs by IUPred2A and compared the score distribution with those of all tardigrade proteins. As expected, unstructured proteins were significantly enriched in T-DRYPs ($p < 2.2e-16$, Wilcoxon rank sum test; Fig 1C). We assigned *Drosophila melanogaster* orthologs for tardigrade proteins and performed enrichment analysis of PANTHER Protein class or Gene Ontology term in T-DRYPs. The results revealed that ribosomal proteins and actin-related cytoskeletal proteins were well concentrated in T-DRYPs (Figs 1D and S2). Among T-DRYPs, however, 105 (31%) proteins had no apparent fly orthologs and T-DRYPs contain many tardigrade-unique proteins (21%) including known tolerance proteins like CAHS proteins (S1 Data). Therefore, we expanded the enrichment analyses to the previously annotated tardigrade tolerance protein families that contain more than 5 members [16] and revealed the significant enrichment of CAHS, LEA, HSP20, HSP70, and peroxiredoxin families in T-DRYPs ($p < 0.01$, chi-square test; Fig 1E and S2 Data), suggesting that our new screening scheme concentrates desiccation-tolerance related proteins to the resolubilized fraction. To evaluate this possibility further, we classified T-DRYPs into 3 groups: stress-up-regulated groups, stress-down-regulated groups, and the others. *R. varieornatus* is one of the toughest tardigrade species that constitutively expresses stress-related genes [16]. Thus, we utilized gene expression data of 2 closely related tardigrades, *Hypsibius exemplaris* and *Paramacrobiotus metropolitanus* (formerly *Paramacrobiotus* sp. TYO), both of which exhibit strong up-regulation of tolerance gene expression upon desiccation [11,17,31]. Of 336 T-DRYPs, 315 proteins had orthologs in both species and 72 genes were up-regulated during dehydration (Fig 1F and S1 Data). Statistical analysis indicated that the up-regulated proteins were significantly enriched in T-DRYPs compared with the tardigrade proteome ($p = 9.53e-29$, chi-square test; S2 Data). In addition, the up-regulated proteins also exhibited a much higher unstructured score (Fig 1G), suggesting that tolerance-related unstructured proteins were well concentrated in the resolubilized fraction in our scheme. Because CAHS proteins were highly enriched in the T-DRYPs (Fig 1E), and also 3 major bands in the resolubilized fraction were separately identified as CAHS12, CAHS3, and CAHS8 (Figs 1B and S3), we focused on these 3 CAHS proteins for further analyses.

CAHS3, CAHS8, and CAHS12 reversibly assemble into filaments or granules in animal cells depending on hyperosmotic stress

To visualize the stress-dependent condensation, 3 CAHS proteins, such as CAHS3, CAHS8, and CAHS12 proteins were separately expressed as a GFP-fused protein in human cultured HEp-2 cells and the distribution changes of these fusion proteins were examined upon exposure to a hyperosmotic stress, which induces water efflux like dehydration stress [32]. In an

unstressed condition, CAHS3-GFP broadly distributed in the cytosol, whereas CAHS8-GFP and CAHS12-GFP distributed broadly in both the cytosol and the nucleus with CAHS12-GFP showing a slight preference for the nucleus (Fig 2A). When exposed to hyperosmotic medium supplemented with 0.4 M trehalose, CAHS3-GFP condensed and formed a filamentous network in the cytosol (Fig 2A and 2B). Similar filament formation was observed when CAHS3 alone was expressed without GFP (S4 Fig), suggesting that filament formation is an intrinsic feature of CAHS3 protein rather than artifact of fusion with GFP. CAHS12-GFP also formed filaments in the cytosol and more prominently in the nucleus in a majority of cells, though granule-like condensates were also observed in the nucleus of approximately 34% of the cells (Figs 2B and S5). CAHS8-GFP predominantly formed granule-like condensates especially in the nucleus, but filaments were also observed in the cytosol in a small population (approximately 3%) of the cells. Similar distribution changes were observed even when GFP was fused to the opposite site in CAHS proteins (S6 Fig), while GFP alone did not exhibit such drastic changes. When hyperosmotic stress was removed by replacing with isosmotic medium, all CAHS condensates, both filaments and granules, rapidly dispersed (Fig 2A and 2B). Hyperosmotic stress by other supplemented osmolytes, such as 0.2 M NaCl or 0.4 M sorbitol, which have an equivalent osmolarity to 0.4 M trehalose, induces similar filament or granule formation, suggesting that the hyperosmotic stress itself is the driver of condensation rather than specific effects of each osmolyte (S7 Fig). Similar reversible condensations of CAHS proteins were also observed when expressed in *Drosophila* cultured S2 cells (S8 Fig and S1 Movie), indicating that the stress-dependent filament/granule condensations are intrinsic features of CAHS proteins commonly observed in animal cells of taxonomically distant species.

Granule-like condensates of CAHS8 resemble droplet structures formed by intrinsically disordered proteins via liquid–liquid phase separation. To test this possibility, we examined the effect of 1,6-hexanediol, a disruption reagent of liquid-like condensates. After treatment with 5% 1,6-hexanediol for 30 min, the well-known droplet-forming protein FUS effectively dispersed, while several CAHS8 granules in the nucleus also dispersed but much less effectively than FUS protein granules (S9 Fig), suggesting that CAHS8 granules were partly liquid like. In contrast, the filament structures of CAHS3 or CAHS12 were not affected by the hexanediol treatment, suggesting that CAHS3 and CAHS12 filaments were in a static solid-like state. To further assess the staticity of CAHS filaments, we performed fluorescence recovery after photobleaching (FRAP) analysis on CAHS3-GFP both before and after exposure to hyperosmotic stress. In unstressed cultured cells, CAHS3-GFP was broadly distributed in the cytosol and the bleached fluorescence was rapidly recovered (Fig 2C), indicating their high mobility nature. In contrast, under hyperosmotic stress, CAHS3-GFP filaments exhibited almost no fluorescence recovery after bleaching (Fig 2D), suggesting that CAHS3 proteins formed static filaments in response to a hyperosmotic stress. The filamentous networks formed by CAHS proteins resembled cytoskeletal structure. To examine possible cooperation between CAHS filament formation and other cytoskeletal structures or organelles, we performed co-localization analyses and observed no co-localization between filament-forming CAHS proteins and any examined intracellular structures except for slight co-localization with actin filaments (Figs 2E and S10A–S10C). GFP alone also exhibited slight co-localization with actin filaments and actin polymerization inhibitor did not disrupt filament formation of CAHS3 and CAHS12 proteins (S10D, S10E, and S11 Figs), suggesting that CAHS filament formation is also independent from actin filaments. These results suggested that CAHS molecules freely disperse in an unstressed condition, but upon the exposure to hyperosmotic stress, CAHS molecules are firmly integrated into an additional cytoskeleton-like filaments.

To elucidate the process of filament formation and deformation in more detail, we captured time-lapse images of cells expressing CAHS3-GFP while changing the stress conditions by

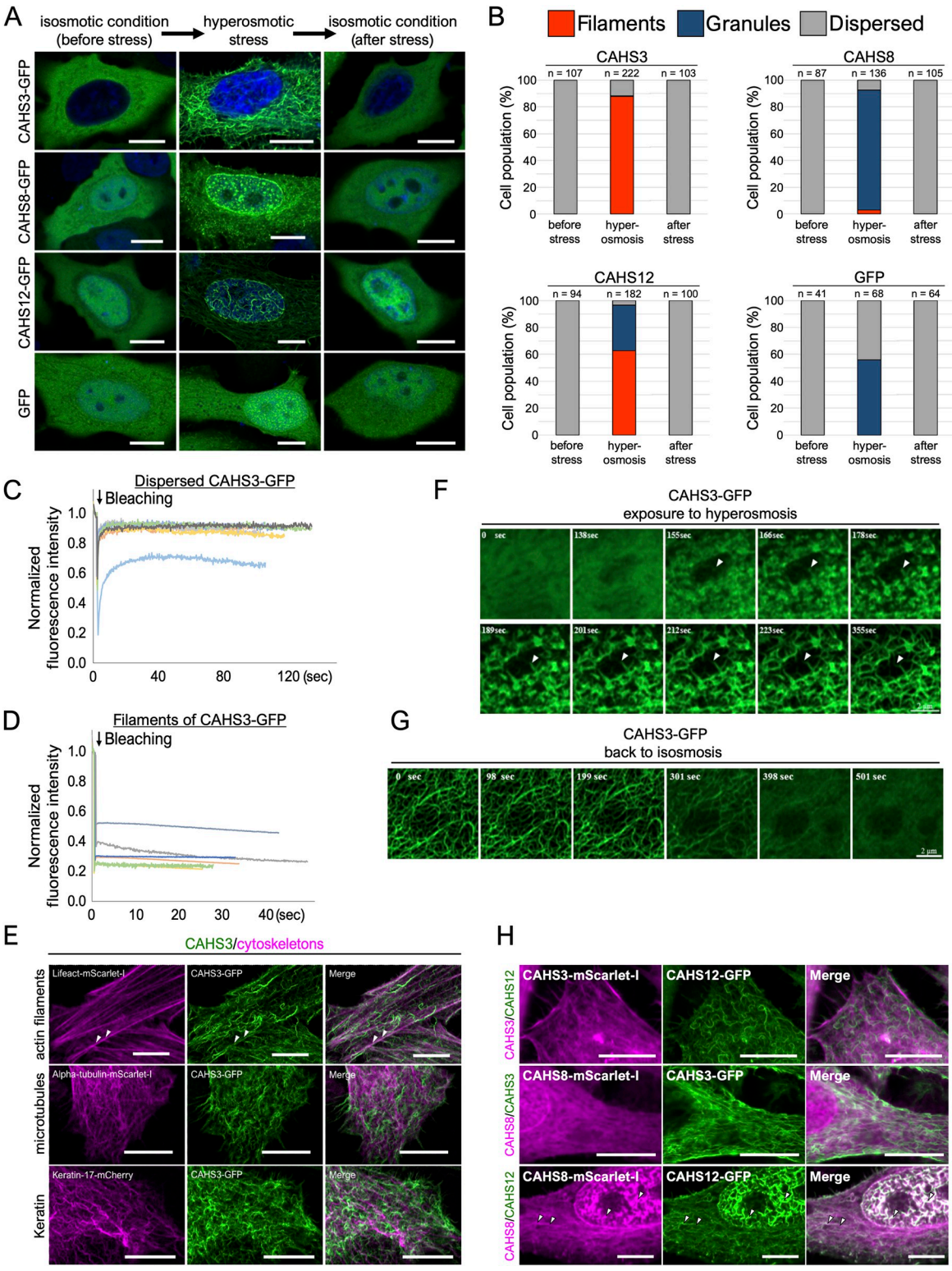

Fig 2. Reversible formation of filaments or granules by CAHS3, CAHS8, and CAHS12 proteins in response to a hyperosmotic stress. (A) Distribution changes in AcGFP1-tagged CAHS3, CAHS8, or CAHS12 proteins in HEp-2 cells during the transient hyperosmotic treatment with HBSS containing 0.4 M trehalose. Blue indicates Hoechst33342 staining of nuclei. (B) The proportion of distribution patterns (filaments, granules, or dispersed) of each CAHS protein in human cells. (C and D) FRAP analyses of CAHS3-GFP in human cells in dispersed state under an isosmotic condition (C, $n = 7$) and in a filament-formed state under a hyperosmotic condition

(D, $n = 6$). (E) Confocal images of AcGFP1-tagged CAHS3 proteins and fluorescently labeled cytoskeletal proteins in HEp-2 cells under a hyperosmotic condition. White arrowheads indicate slight co-localization of CAHS3 proteins and actin filaments. (F and G) Time-lapse images of filament formation or deformation of CAHS3-GFP in human cells (see also S2 and S3 Movies). CAHS3-GFP first condensed into granules (155 s) and then elongated into filaments (355 s) as indicated by white arrowheads (F). CAHS3-GFP filaments simultaneously collapsed and dispersed (398 s) (G). Time since the medium exchange to hyperosmotic (F) or isosmotic (G) solution is shown in each image. (H) Fluorescent images of HEp-2 cells co-expressing pairs of CAHS3, CAHS8, and CAHS12 proteins with a different fluorescent-tag under a hyperosmotic condition. CAHS3 co-localized with neither CAHS8 nor CAHS12. In contrast, CAHS8 well co-localized with CAHS12 filaments. White arrowheads indicate representative co-localization. Scale bar, 10 μm in (A, E, and H), 2 μm in (F and G). The underlying numerical data are available in S4 Data (B–D). CAHS, cytoplasmic-abundant heat-soluble; FRAP, fluorescence recovery after photobleaching; HBSS, Hanks' Balanced Salt Solution.

https://doi.org/10.1371/journal.pbio.3001780.g002

high-speed super-resolution microscopy. Approximately 2.5 min after the medium was changed to a hyperosmotic condition by a perfusion device, CAHS3-GFP began to condense simultaneously at many sites in the cells and rapidly formed fibril structures. The fibrils then further extended in a few dozen seconds (Fig 2F and S2 Movie). When the hyperosmotic stress was removed by changing to an isosmotic medium, CAHS3 filaments simultaneously began to loosen and gradually dispersed in approximately 6 min (Fig 2G and S3 Movie). The initial condensation of CAHS3 and the granule formation of CAHS8 likely occurred via phase separation, which frequently leads to co-condensation of multiple proteins, especially those containing similar motifs [33]. CAHS proteins share several conserved motifs and could thus cooperatively form the same condensates. To examine this, we co-expressed pairs of the 3 CAHS proteins labeled with different fluorescent proteins in human cells. Under hyperosmotic stress, CAHS3 filaments did not co-localize with CAHS8 granules or CAHS12 filaments (Fig 2H). In contrast, CAHS8 largely co-localized with CAHS12 filaments throughout the cell, suggesting that the granule-forming CAHS8 cooperatively forms the filament structure with other CAHS proteins such as CAHS12.

Secondary structure in the conserved C-terminal region is responsible for CAHS filament formation

To reveal the structural basis of CAHS filament formation, we first performed de novo motif search and found 10 conserved motifs by comparing 40 CAHS proteins of 3 tardigrade species, *R. varieornatus*, *H. exemplaris*, and *P. metropolitanus* (S12 and S13 Figs and S3 Data). In particular, we found that 2 C-terminal motifs (CR1 and CR2) are highly conserved in all CAHS family members except 1 CAHS protein of *H. exemplaris* (S12 Fig). To determine the region responsible for filament formation, we generated a series of truncated mutant proteins of CAHS3 or CAHS12 either N-terminally or C-terminally, and examined their filament formation in human cultured cells under a hyperosmotic stress (Figs 3A, 3B, and S14). In CAHS3, N-terminal deletion to motif 3 or C-terminal deletion to CR2 drastically impaired filament formation and instead granule formation was frequently observed in the cytosol (Figs 3B, S15A and S15B). Accordingly, we designed a truncated mutant consisting of the minimum required region from motif 3 to CR2 (motif 3-motif H1-CR1-CR2) and revealed that this region is sufficient for the filament formation by CAHS3 protein (Figs 3B and S15C). Similarly, in CAHS12 protein, the region consisting of CR1, CR2, and the 2 preceding motifs (motif H2-motif H3-CR1-CR2) was shown to be necessary and sufficient for the filament formation (S14 Fig). These results indicated that 2 highly conserved motifs (CR1 and CR2) and 2 preceding motifs (65 to 85 residues) play an essential role in the filament formation of both CAHS3 and CAHS12 proteins.

In these identified regions responsible for the filament formation, extensive helix and coiled-coil structures were predicted by the secondary structure prediction tool, JPred4 and COILS (Figs 3C and S16). The coiled-coil structure is the key structural basis for the

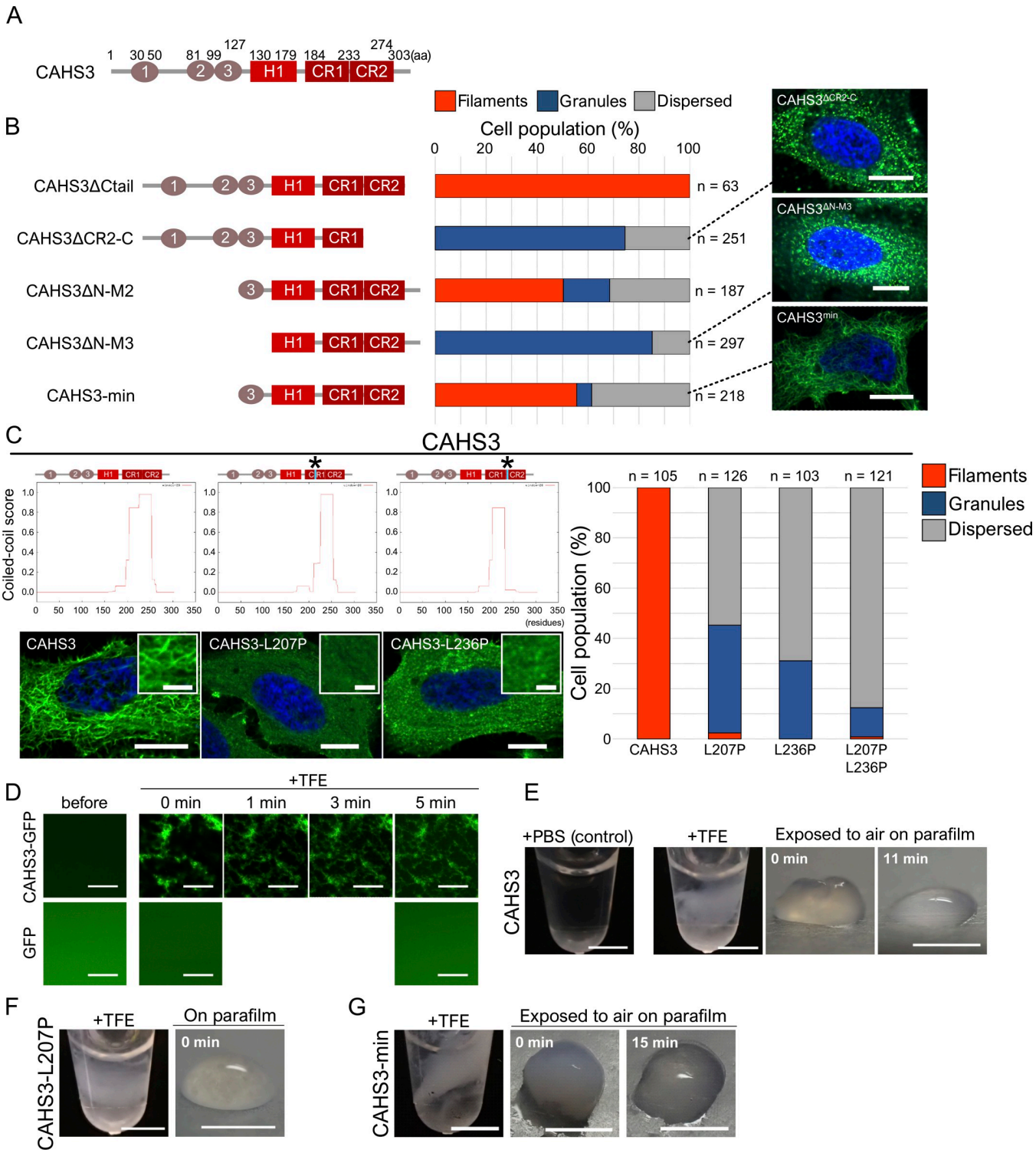

Fig 3. Secondary structure in the conserved C-terminal region is responsible for the CAHS filament formation and gelation. (A) Schematic diagrams of CAHS3 proteins. "CR1" and "CR2" indicate putative helical motifs highly conserved among almost all CAHS family members. "H1" indicate putative helical conserved motifs; "1," "2," and "3" indicate other conserved motifs. (B) Schematic diagrams and the corresponding distribution patterns of the truncated mutants of CAHS3. Quantified cell proportions of the distribution patterns under a hyperosmotic condition are shown as a stacked bar graph. Confocal images are shown for the representative distribution pattern of the corresponding CAHS mutants. Blue indicates Hoechst33342 staining of nuclei. (C) Effects of a helix-disrupting mutation by substituting leucine with proline on filament formation of CAHS3. Schematic structure and the coiled-coil score predicted by COILS are shown for both wild-type and proline substitution mutants. Asterisks indicate the sites of proline substitutions. Substitution with proline

substantially decreased the coiled-coil score in the corresponding region. Confocal images show representative distribution patterns of the corresponding CAHS proteins. Enlarged image is shown as superimposition in each panel. Blue indicates Hoechst33342 staining of nuclei. Quantified cell proportions of each distribution pattern are shown as stacked bar plots on the right. (D) In vitro time-lapse confocal images of fibril formation of CAHS3-GFP proteins (1.24 mg/mL) after adding TFE (final 20%). GFP is a non-filament forming control. (E) TFE-dependent reversible gel-formation of CAHS3 proteins. By adding TFE (final 20%), CAHS3 protein solutions (4.0 mg/mL) became turbid and transited into a gel-like state. The gels spontaneously liquefied within several minutes (shown in white letters) after exposure to air. (F) Filament-impaired CAHS3-L207P mutant protein solutions failed to transit into a gel-like state under 20% TFE. (G) Minimum filament-forming CAHS3 truncated protein (CAHS3-min) solution reversibly solidified under 20% TFE like full-length CAHS3 protein. Scale bar, 10 μm in (B and C), 2.5 μm in superimposition in (C), 20 μm in (D), 2 mm in (E–G). The underlying numerical data are available in S4 Data (B and C). CAHS, cytoplasmic-abundant heat-soluble; TFE, trifluoroethanol.

https://doi.org/10.1371/journal.pbio.3001780.g003

polymerization of IFs [34]. To test the contribution of these predicted secondary structures in filament formation, we generated 2 mutants for each CAHS3 and CAHS12 by substituting leucine with proline, which are predicted to disrupt the helical and coiled-coil structures of CR1 or CR2, respectively (Figs 3C and S17) [35]. As expected, all coiled-coil disruption mutants exhibited significantly impaired filament formation and instead formed granules (Figs 3C and S17–S19). The double mutation (CAHS3-L207P-L236P) further suppressed filaments formation and even reduced granule formation (Figs 3C and S20). These results suggested that the secondary structures of both CR1 and CR2 are an important basis for the filament formation of CAHS3 and CAHS12 proteins.

In vitro reversible gel transition of CAHS proteins depending on desolvating agent and salt

To examine whether CAHS proteins alone are sufficient to form filaments, we performed in vitro experiments using purified CAHS3-GFP proteins. Under an unstressed condition, the uniform distribution of CAHS3-GFP proteins was observed under a confocal microscope (Fig 3D). When the desolvating agent TFE was added to induce a dehydration-like conformational change as in our initial screening, CAHS3-GFP immediately condensed and formed mesh-like fibril networks after 1 min. This result indicated that CAHS3 proteins alone can sense the changes in the condition and form filaments without the assistance of other proteins.

When TFE was added to the solution containing a higher concentration of purified CAHS3 protein (final 4 mg/mL; S21 Fig), the protein solution immediately became turbid, and the solution was solidified into a gel-like state (Fig 3E). When the CAHS3 gel in the tube was spread onto parafilm, the CAHS3 gel spontaneously liquefied within approximately 10 min. We speculated that volatilization of TFE relieved the desolvating stress, thereby making the CAHS3 gel resoluble. Consistently, washing with TFE-free PBS also redissolved the gelated CAHS3 (S22A Fig). While the control protein BSA was not solidified in the same condition (S22B Fig), CAHS8 and CAHS12 exhibited a similar TFE-dependent reversible gel-transition like CAHS3, but the gel of CAHS8 was much smaller than those of other CAHS proteins (S22C and S22D Fig), suggesting differences in the propensity for gelation among CAHS proteins. We also examined whether other stressors that could emerge during dehydration induce CAHS gelation and revealed that an increased concentration of salt (2 M NaCl) also induced the gel transition of CAHS3 proteins, while a molecular crowding agent (20% polyethylene glycol) caused turbidity, but no gelation (S23 Fig). The salt-induced gel persisted even after exposure to air on parafilm, possibly because salt cannot evaporate (S23A Fig). The granule-forming CAHS8 only formed a very small gel in vitro, implying a possible relationship between the filament-forming ability in cells and the gel-forming ability in vitro. This notion was supported by the fact that the filament-impaired CAHS3-L207P mutant protein failed to form the gel in vitro (Fig 3F). In contrast, minimum CAHS3 protein possessing the filament-forming ability (CAHS3-min) successfully formed the gel in vitro upon the addition of TFE and this

transition was reversible as in full-length CAHS3 (Fig 3G), suggesting that the filament-forming ability underlies the gel transition of CAHS proteins in vitro.

CAHS confers the mechanical resistance against deformation forces on cell-like microdroplets and insect cells

To reveal what the gelation of CAHS proteins provides, we evaluated the effects of CAHS gelation on the mechanical properties of cells using cell-like microdroplets covered with a lipid layer. The elasticity of the microdroplets was examined by measuring the elongation length in a micropipette while aspirating with a certain pressure. Microdroplets containing uniformly distributed CAHS3-GFP exhibited continuous elongation exceeding 50 μm under very small pressure (<<0.5 kPa), indicating that they were not elastic and in a liquid phase (Fig 4A–4C). On the other hand, the addition of salt induced the filament formation of CAHS3-GFP and the corresponding microdroplets exhibited significant elasticity (Young's modulus approximately 2.0 kPa in average), indicating that the CAHS3-GFP droplets gelated and then physically hardened. Microdroplets containing GFP alone were not elastic regardless of the addition of salt (Fig 4B and 4C).

To further determine whether CAHS proteins also stiffen animal cells, we established a *Drosophila* S2 cell line stably expressing CAHS3. S2 cells lack canonical cytoplasmic IFs as tardigrade cells do [24] and thus it would be suitable to measure the effect of CAHS filamentation. Measuring the cell stiffness by atomic force microscope (AFM) revealed that under an unstressed condition, the CAHS3-expressing cells exhibited no significant difference in the elasticity with that of the control cells transfected with empty vector. Under a hyperosmotic condition, control cells exhibited higher elasticity than that in an unstressed condition, but the CAHS3-expressing cells exhibited significantly further higher elasticity than that of the control cells under the same condition ($p < 0.05$; Fig 4D), which is consistent with the results using microdroplets. Hyperosmotic stress reduces the cell volume through osmotic pressures [32]. As CAHS3-expressing cells exhibited higher elasticity under a hyperosmotic condition, they somewhat counteract the osmotic pressure and might resist the cell shrinkage. To examine this possibility, we measured the cell volume changes by exposure to hyperosmotic stress. As shown in Fig 4E, CAHS3-expressing cells retained the cell volume significantly better than the control cells ($p < 0.001$; Fig 4E). These results suggest that under a filament-forming condition, CAHS3 proteins stiffen cells and protect them from deformation stress caused by water-efflux stress. Furthermore, we also examined the effect of CAHS3 on cell viability after exposure to hyperosmotic stress. Cell viability was evaluated by the exclusion of propidium iodide (PI), which is an indicator of cell integrity. Under an unstressed condition, CAHS3 expression did not affect the cell viability, but after 48 h treatment with hyperosmotic stress, CAHS3-expressing cells exhibited the increased cell viability (Fig 4F and 4G). The cell stiffening by CAHS proteins may contribute to the stabilization of cell structure and the survival of cells during the dehydration-like process.

Discussion

Our study provides evidence that CAHS proteins reversibly condense in a stress-dependent manner and form a cytoskeleton-like filamentous network in animal cells or undergo gel-transition in vitro (Figs 2A, 3E, S22C and S22D), and we further demonstrated that the CAHS proteins increase the mechanical strength of cell-like microdroplets and improve the resistance against deformation stress of insect cells (Fig 4). In the previous study, CAHS proteins were suggested to act as a vitrifying agent like trehalose during dehydration based on the shift in DSC [18], but this hypothesis was recently counter-argued with data demonstrating that the

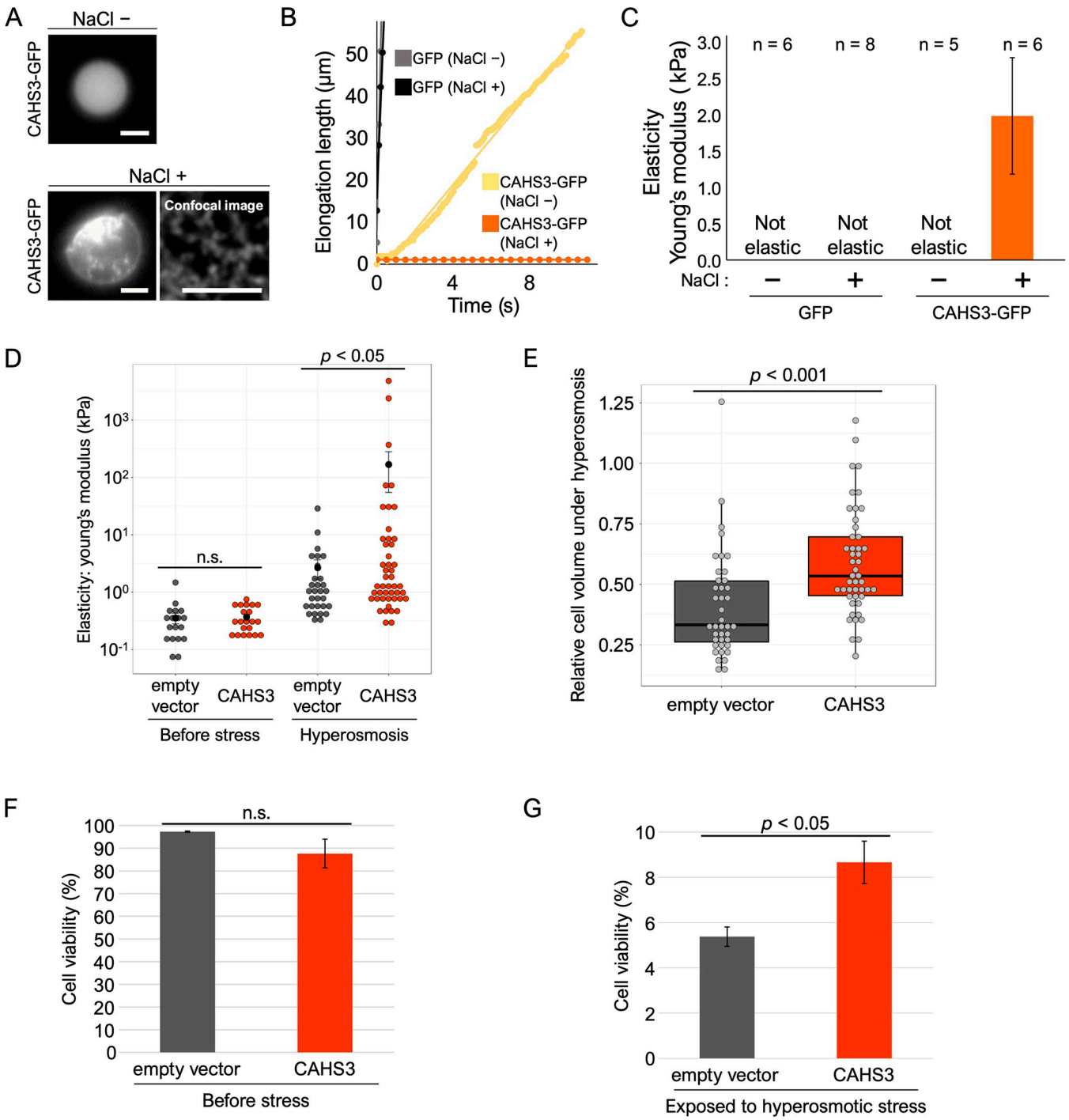

Fig 4. CAHS confers the mechanical resistance against deformation forces on cell-like microdroplets and insect cells. (A) Representative fluorescent images of a microdroplet containing CAHS3-GFP in the absence or presence of additional NaCl. Scale bar, 5 μm. (B) Representative response curves of the elongation length of microdroplets containing CAHS3-GFP or GFP alone under a very small pressure (<<0.5 kPa). Continuous elongation exceeding 50 μm indicates not elastic and in a liquid phase. (C) Comparison of the elasticity (Young's modulus) among droplets containing CAHS3-GFP or GFP with or without NaCl addition. Data are presented as average ± SE. (D) The effects of CAHS3-expression on the cortical elasticity of *Drosophila* S2 cells under hyperosmosis. CAHS3-stably expressing cells exhibited higher elasticity compared to the control cells transfected with empty vector under a hyperosmotic condition supplemented with 0.4 M trehalose for 3 h. Gray and red dots indicate the values of each measurement. Black dots and bars indicate averages and standard errors, respectively. (E) Comparison of cell volume changes by hyperosmotic stress between CAHS3-expressing cells and control cells. The relative cell volume was calculated by dividing the volume under hyperosmotic stress by the averaged cell volume under isosmotic conditions. Center bar and edges indicate 50th, 25th, and 75th percentiles, respectively, and whiskers correspond to the 1.5 interquartile range. (F and G) Comparison of cell viability between

CAHS3-expressing cells and control cells under an isosmotic condition (F) and a hyperosmotic condition for 48 h (G). PI was used to determine dead cells. Survival rates were examined in 6 wells for each condition by counting >500 cells/well. Statistical analyses were performed with the Wilcoxon rank sum test in (D) and (E), and Student *t* test in (F) and (G); n.s. means not significant in the statistical tests. The underlying numerical data are available in S4 Data (B–G). CAHS, cytoplasmic-abundant heat-soluble; PI, propidium iodide.

https://doi.org/10.1371/journal.pbio.3001780.g004

shift in DSC can be explained by water retention of CAHS proteins [21]. Because hydrogel generally has high water retention properties, our observation of gel transition by CAHS proteins supports the water retention in the counterargument rather than vitrification. In vitro gel transition was observed when using a relatively high concentration (approximately 4 mg/mL) of CAHS protein solution (Figs 3E, S22C and S22D), and the filament-impaired CAHS mutants failed in transition to gel (Fig 3F), suggesting that a dense filament formation is the structural basis for the gel transition of CAHS proteins. To confirm the protein concentration used in gel transition in vitro is physiologically relevant, we estimated the amount of endogenous CAHS3 proteins in *R. varieornatus* by immunoblotting analysis, indicating that the amount of CAHS3 proteins is about 3.8 ng per individual (S24 Fig; see Materials and methods). The wet weight of a single individual of *R. varieornatus* was reported to be 1.84 μg [36], which roughly corresponds 1.84 nL, and thus our rough estimate of the concentration of endogenous CAHS3 protein is 2 mg/mL. Considering that CAHS3 proteins are present only in the cytosol and not in the nucleus or extracellular space, the physiological concentration of CAHS3 proteins would be much higher than our estimate, and we assumed it is in a similar range of the concentration used in the gel transition experiments in vitro. Considering the cell volume reduction during dehydration that leads to a significant increase in both the protein concentration and ion strength that might be one of the gel-inducing factors as shown in S23A Fig, the intracellularly abundant CAHS proteins could undergo gel transition in tardigrade cells and provide mechanical stabilization of cell integrity during dehydration (Fig 4C). This gel transition could partly account for the exceptional stability of dehydrated tardigrades. CAHS3-expression also stiffened insect cells, increased the mechanical resistance, and improved hyperosmotic tolerance (Fig 4D–4G). The stress-dependent increase of cell elasticity and the suppression of cell shrinkage under hyperosmosis are in a good agreement with the fact that CAHS3 proteins formed cytoskeleton-like filamentous network in animal cells in a stress-dependent manner and support its functionality, but it is not ascertained whether this enhancement of tolerance fully depends upon the filament formation by CAHS3. CAHS3 might contribute to the tolerance in an alternative way, and our model does not also exclude other possible contributions or functionality of CAHS proteins. The sol-gel transition and filament formation of CAHS proteins were highly reversible and stress dependent, and FRAP analyses revealed that CAHS proteins were immobile only when filaments formed under a stress condition. Therefore, we suppose that CAHS proteins are freely dispersed in a hydrated condition to minimize interference with other biological processes, whereas in a dehydrated condition, CAHS proteins form an intracellular filamentous network and elastic hydrogel to provide mechanical stabilization of cell integrity.

Although CAHS proteins exhibit no sequence similarity with any other cytoskeletal proteins, they formed cytoskeleton-like filamentous networks independently from the other cytoskeleton under a hyperosmotic stress (Figs 2E, S10 and S11) and CAHS-expressing cells exhibited higher resistance against the deformative mechanical forces under the hyperosmotic pressure (Fig 4D and 4E). Hence, CAHS proteins may be a novel cytoskeletal protein family with stress-dependence and gel-forming ability. Although no known motifs are found in the primary sequence of CAHS proteins, the C-terminal region including the highly conserved CR1 and CR2 motifs was essential and sufficient for the filament formation (Figs 3B and S14).

This region was mostly predicted as helical and to form a coiled-coil structure (Figs 3C and S17). This prediction was also supported by the previous circular dichroism (CD) spectroscopy of CAHS1 protein of *R. varieornatus*, another member of the CAHS family [15]. During the review of this manuscript, 2 related papers were published [37,38], which reported that 2 other CAHS proteins, i.e., CAHS1 of *R. varieornatus* and CAHS8 of *H. exemplaris*, formed fibrous structure and gel in a concentration-dependent manner in vitro, and the enriched helix structure in the C-terminal regions in either CAHS proteins were demonstrated by elaborate NMR analyses and/or CD spectroscopy under the condition forming filaments or gels. These recent structural analyses are in a good agreement with our structural predictions (S16 Fig), although the effect of disturbance of such helix structure on filament/gel formation had not been examined. Our observation of the severe impairments in the filament/gel formation by proline substitutions in either the CR1 or CR2 region (Fig 3C and 3F) indicate that the secondary structure of CR1 and CR2 plays important roles in CAHS filament/gel formation. Some intrinsically disordered proteins are reported to form a gel-like granule condensate via promiscuous binding through multivalent interaction sites [39], but in CAHS3 and CAHS12, single amino acid substitution is enough to disrupt both filament formation and gel transition, suggesting that the mechanism of filament/gel formation of CAHS proteins is likely not due to multivalent interactions, but rather to polymerization based on the secondary structure. The prediction of 3D structures by AlphaFold2 [40,41] suggested that CAHS3-min proteins form a helix in the CR1+CR2 region with high confidence (pLDDT = 70 to 90) and 2 CAHS3-min proteins form an antiparallel dimer with the juxtaposition of each helical region where the charge and hydrophobicity distribution is consistent with the stabilization of 2 helix interactions (S25 Fig). This antiparallel alignment is similar to the lamin tetramer formation [34], suggesting that the process of filament formation of CAHS proteins may be somewhat similar to IFs.

In contrast to filament-forming CAHS3 and CAHS12, CAHS8 alone formed granule-like condensates in both human and insect cells under a hyperosmotic condition (Figs 2A and S8). Recently, CAHS1 protein from *R. varieornatus* was also reported to form granules in response to hyperosmotic stress in human cultured cells [37], and these stress-dependent granule condensation by CAHS8 and CAHS1 resembled the stress-granule formation in mammalian cells that occurs through phase separation to create protective membrane-less compartments against stress [42,43]. A recent study revealed that another desiccation tolerance protein, AfrLEA6, which is a group 6 LEA protein of *Artemia franciscana*, also undergoes phase separation to form granules in insect cells [14] and protects enzyme activity from desiccation stress in vitro [44]. Like stress granules and AfrLEA6 granules, CAHS8 granules exhibited certain sensitivity against 1,6-hexanediol treatment (S9 Fig). CAHS8 and CAHS1 might exert similar protective functions via granule condensation under stress conditions. Alternatively, in cells co-expressing CAHS8 and CAHS12, as shown in Fig 2H, CAHS8 contributes to filament formation with CAHS12 in tardigrades.

Intriguingly, the desiccation-induced (up-regulated) tardigrade proteins were significantly enriched in T-DRYPs (S2 Data), implying that our TFE-based isolation scheme could selectively capture the dehydration-responsive proteins that reversibly condense in response to desiccation stress. Two well-known desiccation-tolerance protein families, LEA and CAHS proteins, were also captured as highly enriched in T-DRYPs (Fig 1E). These 2 protein families are largely unstructured in hydration and mutually unrelated in the primary sequence, but both become helix-rich structure upon dehydration [12,37]. TFE is also known as a stabilizer of helical structure [45], for which several stabilization mechanisms have been proposed, e.g., the destabilization of the interaction between polypeptides and water molecules promotes local intramolecular hydrogen bonding in polypeptides and consequently stabilize the helical structure [27,28,46]. Our T-DRYPs isolation method could capture CAHS and LEA proteins

through TFE-induced helix formation as occurred in a dehydrating condition. We also cannot exclude the possibility that some proteins in T-DRYPs could be isolated through the helix-inducing property rather than the desolvating property of TFE. In the T-DRYPs, stress-related unstructured proteins were enriched (Fig 1G), as well as translational proteins and cytoskeleton-related proteins (Fig 1D). These proteins might be incorporated into stress-dependent condensates like stress granules to be protected from stress. Alternatively, some of them like cytoskeletal proteins might be co-precipitated through entangling with CAHS filaments. Although CAHS proteins are conserved only in eutardigrades, proteins with similar properties might be present in other desiccation-tolerant organisms and may contribute to stress resistance. It is noteworthy that the related animal groups such as heterotardigrades or arthropods also lack the canonical cytoplasmic IFs but excellent anhydrobiotic ability is observed in some selected species such as *Echiniscus testudo* (a heterotardigrade), *Polypedilum vanderplanki* (a sleeping chironomid), and *Artemia* (a brine shrimp) [2,5,6]. These animals might possess another class of stress-dependent filament-forming proteins. Recently, a new heat-soluble protein family termed EtAHS was identified in *E. testudo* [20]. This protein family or other new ones are likely good candidates. Our isolation scheme of T-DRYPs may provide a useful method to identify unstructured proteins that undergo reversible condensation to filaments or granules in a stress-dependent manner from various organisms. CAHS proteins were originally identified by searching for heat-soluble proteins to identify anhydrobiotic protectants in tardigrades [15]. Later, many heat-soluble proteins were identified from humans and flies, dubbed Hero proteins [47], that exhibit no sequence similarity with CAHS proteins but provide stabilization of other proteins as CAHS and LEA proteins do. Similarly, future T-DRYPome analysis may lead to the identification of protective phase-separating proteins even in non-anhydrobiotic organisms.

In the present study, we established a new method to identify proteins that are reversibly condensed in response to desolvating agent and found 336 such proteins from desiccation-tolerant tardigrades. The major components, CAHS3 and CAHS12, were shown to form cytoskeleton-like filaments and elastic hydrogel in a stress-dependent manner. Furthermore, we demonstrated that CAHS3 can confer mechanical resistance against deformation stress on insect cells and enhanced their tolerance to dehydration-like stress. We propose that these CAHS proteins may function as novel stress-dependent and gel-forming cytoskeletal proteins that provide mechanical strength to stabilize cellular integrity during stress. Our data suggested a novel desiccation tolerance mechanism based on filament/gel formation. The isolation scheme established in this study opens the way to identifying such novel stress-dependent cytoskeletal proteins from various organisms.

Materials and methods

Animals

We used the previously established YOKOZUNA-1 strain of the desiccation-tolerant tardigrade *R. varieornatus* reared on water-layered agar plate by feeding alga *Chlorella vulgaris* (Recenttec K. K., Japan) at 22˚C as described previously [36].

Identification of trifluoroethanol-dependent reversibly condensing proteins

Prior to protein extraction, tardigrades were starved for 1 day to eliminate digestive food. Approximately 400 *R. varieornatus* were collected and extensively washed with sterilized Milli-Q water to remove contaminants. Tardigrades were rinsed with lysis buffer, phosphate-

buffered saline (PBS; 137 mM NaCl, 2.7 mM KCl, 10 mM Na_2HPO_4, 1.76 mM KH_2PO_4 (pH 7.4)) containing complete protease inhibitors (Roche) and transferred to a 1.7 mL tube. Tardigrades were homogenized in 20 μL lysis buffer using a plastic pestle on ice. The pestle was rinsed with an additional 20 μL of lysis buffer collected in the same tube. After centrifugation at 16,000 × g for 20 min at 4˚C, the supernatant was recovered as a soluble protein extract. To mimic dehydration stress, the desolvating agent, TFE, was added (final concentration 10%, 20%, or 30%), and the mixture was incubated on ice for 1 h to allow complete induction of condensation. After centrifugation at 16,000 × g for 20 min, the supernatant was removed as a TFE-soluble fraction and the remaining precipitate was washed twice by lysis buffer containing TFE at the same concentration. The washed precipitate was resuspended in lysis buffer without TFE and incubated at room temperature for 30 min to facilitate resolubilization. After centrifugation at 16,000 × g at 4˚C, the supernatant was recovered as a resolubilized fraction. The fractions were analyzed by SDS-PAGE and proteins were visualized using a Silver Stain MS Kit (Fujifilm). Three selected bands were excised and separately subjected to mass spectrometry. Comprehensive identification of T-DRYPs was achieved by shot-gun proteomics of the resolubilized fraction. Briefly, proteins in gel slices or in the fraction were digested with trypsin and fragmented peptides were analyzed by nanoLC-MS/MS. Proteins were identified using MASCOT software (Matrix Science). The mass spectrometry proteomics data have been deposited to the ProteomeXchange Consortium via the jPOST repository with the dataset identifier PXD030241 and can be retrieved at http://proteomecentral.proteomexchange.org/cgi/GetDataset?ID=PXD030241.

In silico structure predictions

The unstructured score of the proteins was calculated by IUPred2A [48]. IUPred2A produces the score for each amino acid position in a protein, and an average value was used as a score for each protein. A de novo protein sequence motif search in CAHS protein families was performed by the motif discovery tool, MEME version 5.0.4 [49] (https://meme-suite.org/meme/tools/meme). The parameters were as follows: (occurrence per sequence = 0 or 1; the maximum number to be found = 10; the motif width = 6 to 50). The secondary structures of CAHS3, CAHS8, and CAHS12 proteins were predicted by Jpred4 [50] (https://www.compbio.dundee.ac.uk/jpred/). The coiled-coil regions of CAHS3 and CAHS12 were predicted by COILS [51] (https://embnet.vital-it.ch/software/COILS_form.html or locally executing the software available at ftp://ftp.ebi.ac.uk/pub/software/unix/coils-2.2/). The 3D structure prediction of the CAHS-min protein homo-dimer was performed by Alphafold2 [41] (https://colab.research.google.com/github/sokrypton/ColabFold/blob/main/AlphaFold2_complexes.ipynb). The 3D structures were visualized with UCSF ChimeraX v.1.2 [52].

Enrichment analysis

To utilize well-annotated information in the model organism *D. melanogaster*, we assigned a *D. melanogaster* ortholog for each *R. verieornatus* protein by a reciprocal BLAST search. We assigned 231 fly orthologs for 336 T-DRYPs and 7,361 fly orthologs for all 19,521 *R. varieornatus* proteins. Using the assigned fly orthologs, we performed enrichment analyses with PANTHER Overrepresentation Test [53] (PANTHER Protein Class version 16.0, Fisher's test; http://pantherdb.org/) and Metascape [54] (GO Cellular Components; https://metascape.org/). The list of fly orthologs for all *R. varieornatus* proteins was used as a reference in the enrichment analyses.

Among tardigrade stress-related proteins described previously [16], 7 protein families containing more than 5 members were selected for the enrichment analysis (S2 Data). Enrichment

of each family in T-DRYPs was statistically examined by Fisher's exact test using R. Enrichment of up-regulated genes was similarly examined except using a chi-square test.

Differential gene expression analysis

Transcriptome data at a hydrated state and a dehydrated state were retrieved from the public database (DRR144971-DRR144973 and DRR144978-DRR144980 for *Paramacrobiotus metropolitanus*; SRR5218239-SRR5218241 and SRR5218242-SRR5218244 for *Hypsibius exemplaris*, respectively). The genome sequence of *P. metropolitanus* was retrieved from the public database under accession numbers BHEN01000001-BHEN01000684 [11]. The genome sequence of *H. exemplaris* v3.0 was retrieved from http://www.tardigrades.org. RNA-seq reads were mapped to the genome sequence using HISAT2 v.2.1.0 [55]. Read counts for each gene region were quantified by featureCounts in SubRead package v.1.6.3 [56] and statistically compared by R package DESeq2 [57]. The genes with FDR < 0.01 were considered as differentially expressed genes. Orthologous gene relationships were determined by reciprocal BLAST searches among 3 tardigrade species.

Cell lines

We obtained Hep-2 cells (RCB1889) from RIKEN BioResource Center (BRC). The identity of the cell line was validated by short tandem repeat profiling and the cell line was negative for mycoplasma contamination (RIKEN BRC). The cell was maintained in minimum essential medium (Nacalai Tesque) containing 10% fetal bovine serum (FBS, Cosmo Bio or BioWest) at 37˚C, 5% CO_2. *Drosophila* S2 cells (Gibco) were cultured at 28˚C in Schneider's *Drosophila* Medium (Gibco) supplemented with 10% heat-inactivated FBS (BioWest) and penicillin-streptomycin mixed solution (Nacalai Tesque).

Plasmids

CAHS3, CAHS8, and CAHS12 coding sequences were amplified from the corresponding EST clones of *R. varieornatus* [16] and inserted into pAcGFP1-N1 or pAcGFP1-C1 (Clontech) with $(GGGGS)_3$ linker using In-Fusion HD Cloning Kit (Takara). Plasmids to express CAHS deletion mutants (CAHS3Δctail, CAHS3ΔCR2-C, CAHS3ΔN-M2, CAHS3ΔN-M3, CAHS3-min, CAHS12Δctail, CAHS12ΔCR2-C, CAHS12ΔN-M1, CAHS12ΔN-H2, and CAHS12-min) or leucine-to-proline substitution mutants (CAHS3-L207P, CAHS3-L236P, CAHS3-L207P-L236P, CAHS12-L204P, and CAHS12-L241P) were generated by inverse PCR and ligation or PCR-based site directed mutagenesis. The CAHS3/8/12-mScarlet-I expression vector was generated from CAHS3/8/12-GFP expression vector by replacing AcGFP1 coding sequences with *mScarlet-I* sequence fragments [58] synthesized artificially (IDT). Expression constructs for various cytoskeleton or organelle marker proteins were obtained from Addgene (S1 Table). For bacterial expression of His_6-tagged CAHS proteins, *CAHS3*, *CAHS8*, or *CAHS12* coding sequences were amplified and inserted into pEThT vectors [15], and *CAHS3-GFP* was similarly inserted into a pCold-I vector (Takara). For expression in *Drosophila* cells, codon-optimized *CAHS3*, *CAHS8*, *CAHS12*, and *AcGFP1* DNA fragments were synthesized (Gene Universal) and inserted into pAc5.1/V5-His A vector (Invitrogen). The FUS-Venus plasmid was a kind gift from Dr. Tetsuro Hirose.

Live cell imaging under hyperosmosis

We used Hep-2 cells for live-imaging of fluorescently labeled proteins because Hep-2 cell were well sticky even under a stress condition and enabled precise inspections. Hep-2 cells were

transiently transfected with an expression vector of fluorescently labeled proteins using Lipofectamine LTX & Plus Reagent (Invitrogen) for 48 h before stress exposure. Prior to microscopy, the medium was replaced with Hanks' Balanced Salt Solution (HBSS) without the dications and phenol red. For exposure to hyperosmotic stress, the buffer was replaced with HBSS containing 0.4 M trehalose. The cells were stained with Hoechst 33342 (5 μg/mL, Lonza) to visualize nuclear DNA. Fluorescent signals were observed using a confocal microscope LSM710 (Carl Zeiss). The number of cells for each CAHS distribution pattern, such as dispersed, granules, or filaments, were counted by 2 independent investigators and averaged counts were used. For time-lapse imaging in 3D space, we used the LSM-980 with Airyscan to perform super-resolution imaging. From the z-stack images, we generated orthogonal projections using ZEN 2.6 software. In time-lapse imaging experiments, a perfusion system KSX-Type1 (Tokai Hit) was used to replace the buffer. To visualize actin filaments by chemical staining, Hep-2 cells were treated with silicon-rhodamine dye probing actin (SiR-actin, Spirochrome) in HBSS containing the drug efflux inhibitor verapamil (10 μM, Tokyo Chemical Industry) for 2 h. For actin polymerization inhibition experiments, cells were treated with cytochalasin B (5 μM, Nacalai Tesque) for 60 min. Cells were then observed by a confocal microscope LSM-710 (Carl Zeiss).

Fluorescence recovery after photobleaching (FRAP) analysis

Hep-2 cells were transiently transfected with the expression construct of CAHS3-GFP. The transfected cells were then exposed to isosmotic HBSS or hyperosmotic buffer, HBSS containing 0.4 M trehalose, to analyze the mobility of CAHS3-GFP in the dispersed or filament state, respectively. FRAP experiments were performed at room temperature using a confocal fluorescence microscope (FV1200, Olympus). A spot approximately 0.77 μm in diameter was photobleached at 100% laser power (wavelength 473 nm), and the fluorescence recovery curves were analyzed using the Diffusion Measurement Package software (Olympus). The fluorescence intensity was normalized by the initial intensity before photobleaching.

Sensitivity to 1,6-hexanediol treatment

Hep-2 cells were transfected with expression vectors of CAHS3/8/12-AcGFP1 or FUS-Venus. After 48 h, cells were exposed on minimum essential medium supplemented with 0.4 M trehalose and 10% FBS for 1 h to induce the formation of granules or filaments. FUS protein was used as a control as it is known to be incorporated into liquid droplets under hyperosmosis [59]. After the addition of a liquid droplet disruptor, 1,6-hexanediol (final 5%), fluorescent images were captured at 0 and 30 min later by a confocal microscope LSM710 (Carl Zeiss). The fluorescence intensity was measured by Fiji and normalized to the initial fluorescence intensity of the granules or filaments.

Immunofluorescence

Hep-2 cells expressing CAHS3 or CAHS3 mutants were exposed to HBSS containing 0.4 M trehalose for 60 min to induce filament formation. The cells were then fixed in methanol at −30˚C for 3 min and washed 3 times with PBS containing 0.1% Tween 20 (PBS-T). The cells were blocked with 2% normal goat serum (Abcam) for 1 h at room temperature and then reacted with 1/200 diluted antiserum against CAHS3 in 2% normal goat serum for 1 h at room temperature or 16 h at 4˚C. The cells were washed 3 times with PBS-T and then reacted with 1/1,000 diluted Alexa Fluor546 goat anti-guinea pig secondary antibody (Invitrogen) and 1 μg/mL DAPI in 2% normal goat serum for 1 h at room temperature. Fluorescent signals were observed using a confocal microscope LSM710 (Carl Zeiss).

Protein preparation

Recombinant proteins were expressed as N-terminally His_6-tagged proteins in *Escherichia coli* BL21(DE3) strains. CAHS3, CAHS8, and CAHS12 proteins were expressed using pET system (Novagen) essentially as described previously [15]. CAHS3-GFP and AcGFP1 were expressed using a cold shock expression system (Takara) essentially as described previously [60]. Bacterial pellets were lysed in PBS containing complete EDTA-free protease inhibitors (Roche) by sonication. For CAHS3, CAHS8, and CAHS12, the supernatant was heated at 99˚C for 15 min to retrieve heat-soluble CAHS proteins in a soluble fraction as described previously [15]. From the soluble fraction, His_6-tagged proteins were purified with Ni-NTA His-Bind Superflow (Novagen) and dialyzed against PBS using a Pur-A-Lyzer Midi Dialysis Kit (Merck).

In vitro polymerization of CAHS3-GFP proteins

Purified CAHS3-GFP or AcGFP1 protein solution in PBS (approximately 40 μM) was directly dropped on cover glass (MATSUNAMI), and fluorescent images were captured by a confocal microscope LSM710 (Carl Zeiss). To induce the polymerization of CAHS3, an equal amount of PBS containing TFE was added (final 20%), and time-lapse images were captured every 5 s.

In vitro gelation

Purified recombinant CAHS protein solution (5 mg/mL) was placed in a 0.2-mL tube. Inducing reagents such as TFE (final 20%), polyethylene glycol (final 20%), or NaCl (final 2 M) were added to the protein solution and incubated at room temperature for 10 min. Then, the tube contents were spread out on parafilm to check if it had solidified into a gel-like state or remained in a liquid state. Photos were obtained by a digital camera with a short focal length (Olympus TG-6).

Preparation of cell-like microdroplets

Cell-like microdroplets coated with a lipid layer of phosphoethanolamine (Nacalai Tesque) were prepared in an oil phase. First, dry films of the lipids were formed at the bottom of a glass tube. Mineral oil (Nacalai Tesque) was then added to the lipid films followed by 90 min of sonication. The final concentration of the lipid/oil solution was approximately 1 mM. Next, 10 vol % of the protein solution (40 μM GFP-labeled CAHS3 or 40 μM GFP) was added to the lipid/oil solution at approximately 25˚C. After emulsification via pipetting, approximately 40 μL sample containing the microdroplets was placed on a glass-bottom dish. To condense the proteins inside the droplets upon dehydration, we added 40 μL salted oil. Mechanical measurements were performed 90 min after the droplet volume was approximately halved. For fluorescent imaging, 21 μM CAHS3-GFP and 171 μM CAHS3 were mixed and used.

Measurement of the elasticity of droplets by micropipette aspiration

The elasticity of the cell-like microdroplets was evaluated by a micropipette aspiration system as reported previously [61]. The surface elasticity (Young's modulus), E, is derived from the linear relationship between the elongation length into the micropipette, ΔL, and the aspiration pressure, ΔP: $E = (3\Delta P R_p \Phi/2\pi)/\Delta L$, wherein R_p and Φ are the micropipette inner radius and wall function, which is derived from the shape of the micropipette. We used a micropipette with an R_p smaller than × 0.4 of the microdroplet radius R. The value of Φ is 2.0. An increase in ΔL to above 50 μm under a very small ΔP ($<<$0.5 kPa) indicates that the microdroplet is in liquid phase. In the case of the elastic gel phase, a linear relationship between ΔL and ΔP was

confirmed for the small deformation within $\Delta L < 5$ μm and $\Delta P < 3$ kPa. Under these conditions, we derived the values of E. The temperature was approximately 25˚C.

Establishment of stably transfected cell line of *Drosophila* S2 cells

The expression vector Ac5-STABLE2-neo was obtained from Addgene (#32426) [62], and then the coding sequence of FLAG-mCherry was replaced with the codon-optimized CAHS3 coding sequence (Gene Universal) to express CAHS3-T2A-EGFP-T2A-neoR under the control of Ac5 promoter. The empty vector was constructed by deleting FLAG-mCherry from Ac5-STABLE2-neo, which was designed to express T2A-EGFP-T2A-neoR driven by the same Ac5 promoter. *Drosophila* S2 cells were transfected using a cationic liposome reagent Hilymax (Dojindo) with the expression construct or the empty vector above. We established stably transfected cells by culturing for 6 weeks under the drug selection with G418 disulfate (2,000 μg/mL, Nacalai Tesque).

AFM measurement of elasticity of S2 cells expressing CAHS3 protein

Drosophila S2 cells stably transfected with the CAHS3 expression construct and empty vector were cultured on PLL-coated coverslips (MATSUNAMI) at least 1 day before the measurement for cell attachment. For hyperosmotic treatment, the culture medium was replaced with the one containing 0.4 M trehalose 1 h before the measurement. The force spectroscopy was conducted using NanoWizard 3 Ultra AFM (Bruker) with an inverted microscope Olympus IX70 at 22˚C. Cantilevers BL-AC40TS (Olympus) with a nominal spring constant of 0.09 N/m was calibrated using the thermal noise method for each experiment. Photodetector sensitivity was determined by fitting a line to the slope of the force distance curve acquired on the glass substrate. Indentation tests were performed at the speed of 2 μm/s for both approach and retraction, and the tests were repeated 16 times for each single cell. Young's moduli of the cells were obtained by fitting the Hertz model to the force curves using indentation depths <1 μm.

Measurement of cell volume

The volume of each cell was measured using serial images of optical sections according to the previous publication [63]. Three-dimensional imaging was performed for GFP fluorescence in the stably transfected cells at 1.05 μm z-axis intervals using a 63 × /1.2 oil-immersion lens on a confocal microscope LSM710 (Carl Zeiss). Cross-sectional area of the cell was calculated from each sectioned image using Fiji software, and cell volume was estimated as a sum of them.

Cell viability assay

As a hyperosmotic treatment, the S2 cells were exposed to the culture medium containing 0.4 M trehalose for 48 h. The cells were stained with Hoechst33342 (6.7 μg/mL, Lonza) and PI (0.67 μg/mL, Dojindo) for 30 min and observed with a fluorescence microscope BZ-X810 (Keyence). Hoechst33342-positive and PI-negative cells were counted as live cells and double-positive cells were counted as dead cells. The survival rates were calculated in 6 wells for each condition by counting 500 to 700 cells/well using analysis software Hybrid Cell Count (Keyence).

Estimation of the amount of endogenous CAHS3 protein by immunoblotting

After extensive washing with purer water, approximately 100 *R. varieornatus* were lysed using pestle in 30 μL PBS containing complete EDTA-free protease inhibitors (Roche) and

centrifuged at 16,000 × g for 10 min. The soluble fractions of tardigrade lysate were mixed with 5 × SDS sample buffer (62.5 mM Tris-HCl (pH6.8), 25% glycerol, 10% sodium dodecyl sulfate, and 0.01% bromophenol blue) and 2-mercapto-ethanol. After heated at 100˚C for 3 min, the samples were resolved by SDS-PAGE analysis and electroblotted onto PVDF membrane (Millipore). The membrane was blocked with 1% normal goat serum (Abcam) for 1 h at room temperature and reacted with the affinity-purified CAHS3 antibody diluted by 1% normal goat serum for 1 h at room temperature. After washed with TBS-T 3 times, the membrane was reacted with diluted peroxidase labeled anti-rabbit IgG antibody (KPL) for 1 h at room temperature. The membrane was washed with TBS-T 3 times, and then antibody-antigen complex was detected by ImageQuant LAS 500 (Cytiva) using enhanced chemiluminescence system (GE Healthcare). The diluted series of recombinant CAHS3 proteins (2.5, 5.0, 10.0, 20.0, 40.0 ng) were analyzed simultaneously on the same blot as quantification standards. Signal intensity of each corresponding band was measured by Fiji software and a linear regression was used to generate a standard curve between the signal intensity and the amount of protein as [Signal intensity] = [Amount of protein (ng)] × 446595.3952–696903.625; $R^2 = 0.9962$. Using the well-fitted standard curve, the amount of endogenous CAHS3 protein was calculated to be approximately 3.81 ng per tardigrade.

Supporting information

S1 Fig. Silver-stained gel images of each fraction in the T-DRYP isolation process. Each fraction was analyzed by SDS-PAGE and visualized by silver-staining. The image of the resolubilized fraction is partly presented in Fig 1B. As the concentration of TFE increased (0% to 20%), proteins decreased in the TFE soluble fraction, and proteins increased in both the irreversible precipitate and the resolubilized fraction. Treatment with 20% and 30% TFE had largely similar effects.
(TIF)

S2 Fig. Enrichment analysis of Gene Ontology (GO) terms in T-DRYPs. Ribosomal proteins and fiber proteins were highly enriched in T-DRYPs. GO terms of cellular components enriched in T-DRYPs were analyzed by Metascape. The numerical data are available in S4 Data.
(TIF)

S3 Fig. Prediction of disordered regions of CAHS3, CAHS8, and CAHS12 proteins. (A–C) The unstructured score of each amino acid residue was calculated by IUPred2A for CAHS3 (A), CAHS8 (B), and CAHS12 (C). Scores above 0.5 indicate that the region is disordered. Each protein was predicted to be largely disordered throughout. The numerical data are available in S4 Data (A–C).
(TIF)

S4 Fig. Hyperosmotic stress-dependent distribution changes in CAHS3 proteins without a GFP-tag in HEp-2 cells. CAHS3 proteins were transiently expressed in HEp-2 cells and detected by immunofluorescence under isosmotic or hyperosmotic conditions. The detected distribution changes were similar to those of GFP-labeled CAHS3. Blue indicates DAPI staining of nuclei. Scale bar, 10 μm.
(TIF)

S5 Fig. Representative images for each distribution pattern (filament, granule, or dispersed) of CAHS3-GFP, CAHS8-GFP, CAHS12-GFP, and GFP alone in human cultured HEp-2 cells. N/A indicates that the corresponding distribution pattern is not or rarely found

in a hyperosmotic condition. Scale bar, 10 μm.
(TIF)

S6 Fig. GFP-fusion to the other end (N-terminus) of CAHS proteins exhibited similar distribution patterns to those of C-terminally GFP-fused CAHS proteins under hyperosmosis. N-terminally GFP-fused CAHS3 and CAHS12 exhibited filament-formation in response to hyperosmotic stress, and CAHS8 formed granule-like condensates like C-terminally GFP-fused CAHS proteins. The GFP-fusion site (N or C-terminus) did not affect the distribution pattern of CAHS proteins.
(TIF)

S7 Fig. Effects of other hyperosmotic stressors (NaCl and sorbitol) on the distribution patterns of GFP-tagged CAHS proteins and GFP alone in human cultured cells. (A–B) Representative distribution patterns of GFP-tagged CAHS proteins and GFP alone under hypertonic medium supplemented with 0.2 M NaCl (A) or hyperosmotic medium supplemented with 0.4 M sorbitol (B). Distribution changes were similar to those observed when treated with 0.4 M trehalose (Fig 2A). Blue indicates Hoechst33342 staining of nuclei. Scale bar, 10 μm.
(TIF)

S8 Fig. Distribution changes of CAHS-GFP proteins in *Drosophila* cultured S2 cells during transient hyperosmotic treatment. Like in human cells, CAHS3-GFP and CAHS12-GFP reversibly formed filaments and CAHS8-GFP reversibly formed granules upon hyperosmotic stress in fly cells. As a hyperosmotic medium, the culture medium containing 0.4 M trehalose was used. Blue indicates Hoechst33342 staining of nuclei. Scale bar, 5 μm.
(TIF)

S9 Fig. Effects of the liquid droplet disruptor, 1,6-hexanediol on condensates of CAHS proteins. (A) Representative confocal images of human cells expressing FUS-venus ($n = 15$), CAHS3-GFP ($n = 7$), CAHS8-GFP ($n = 24$), or CAHS12-GFP ($n = 7$) under hyperosmotic and 1,6-hexanediol stress. Exposure to 1,6-hexanediol for 30 min dispersed FUS and CAHS8 condensates. FUS is a control protein sensitive to 1,6-hexanediol. (B) Box plots show the distributions of the fluorescence intensity at 30 min relative to that at 0 min. CAHS3 and CAHS12 filaments were not unaffected by 1,6-hexanediol. Center bar and edges indicate 50th, 25th, and 75th percentiles, respectively, and whiskers correspond to the 1.5 interquartile range. Scale bar, 10 μm. The underlying numerical data are available in S4 Data (B).
(TIF)

S10 Fig. Co-localization analyses between CAHS proteins and cytoskeletons or organelles. (A–C) Confocal images of HEp-2 cells expressing AcGFP1-tagged CAHS3 (A), CAHS8 (B) or CAHS12 (C) and other fluorescently labeled actin filaments, microtubules, 3 intermediate filaments (keratin, vimentin, and lamin) or 2 organelle markers (endoplasmic reticulum and mitochondria) under hyperosmosis. CAHS filaments or granules did not colocalized with almost all examined intracellular structures, except for vimentin and actin filaments. Although CAHS8 overlapped vimentin filaments (B), tardigrades have no vimentin homologues. White arrowheads indicate detected co-localization. (D and E) Co-localization analyses between intrinsic actin filaments and CAHS-GFP proteins or GFP alone. Actin filaments was visualized by staining with Lifeact-mScarlet-I (D) or the chemical probe SiR-actin (E). All examined GFP-fusion proteins including GFP alone slightly co-localized with actin filaments, suggesting that GFP-moiety causes weak interaction with actin filaments. Scale bar, 10 μm.
(TIF)

S11 Fig. Effects of actin polymerization inhibitor, cytochalasin B on CAHS filaments. Depolymerization of actin filaments had no effects on the formation of CAHS filaments. Scale bar, 10 μm.
(TIF)

S12 Fig. Informatically extracted motif structures of CAHS protein family. Ten conserved sequence motifs were identified by MEME among 40 CAHS proteins from 3 tolerant tardigrades (*Hypsibius exemplaris*, *Paramacrobiotus metropolitanus*, and *Ramazzottius varieornatus*). Each motif is shown in the corresponding colored box. Both CR1 and CR2 were conserved in all 40 CAHS proteins except CR2 in HdCAHS6_2. CR1, CR2, H1, H2, H3, and H4 were predicted as helical regions by JPred4 (S12 Fig). Hd, *H. exemplaris* (formerly *H. dujardini*); Pr, *P. metropolitanus* (formerly *Paramacrobiotus* sp. TYO); Rv, *R. varieornatus*.
(TIF)

S13 Fig. Sequence logo representation of the conserved protein sequence motifs among the CAHS protein family.
(TIF)

S14 Fig. Conserved C-terminal regions are necessary and sufficient for the filament formation of CAHS12. (A) Schematic diagrams of CAHS12 proteins. "CR1" and "CR2" indicate putative helical motifs conserved in CAHS family. "H2," "H3," and "H4" indicate putative helical conserved motifs; "1" and "4" indicate other conserved motifs. (B) Schematic diagrams and the corresponding distribution patterns of the CAHS12 truncated mutants. Blue indicates Hoechst33342 staining of nuclei. Scale bar, 10 μm. The underlying numerical data are available in S4 Data (B).
(TIF)

S15 Fig. Distribution patterns of CAHS3 truncated mutants without GFP-tag in HEp-2 cells under a hyperosmotic condition. (A–C) CAHS3 truncated mutants were expressed in HEp-2 cells and their distribution patterns were detected by immunofluorescence under a hyperosmotic condition. CAHS3ΔCR2-C (A) and CAHS3ΔN-M3 (B) failed to form long filamentous networks, whereas CAHS3-min (C) successfully formed filaments. The detected distribution patterns were similar to those of the corresponding CAHS3 mutants labeled with GFP (Fig 3B). Scale bar, 10 μm.
(TIF)

S16 Fig. Predicted secondary structures of CAHS proteins. Secondary structure predictions by JPred4 are shown for CAHS3 (A), CAHS8 (B), and CAHS12 (C). Red boxes indicate putative helical regions and green arrows indicate putative beta sheet regions in jnetpred, JNETHSSM and JNETPSSM, respectively. Lupas shows coiled-coil prediction; "C" or "c" indicate putative coiled-coil region and the capital "C" indicates a higher probability. JNETSOL show solvent accessibility.
(TIF)

S17 Fig. Suppression of filament-formation by mutations disrupting the coiled-coil structure in the conserved region of CAHS12. Effects of a helix-disrupting leucine to proline substituting mutation on CAHS12 filament formation are shown. Coiled-coil score predicted by COILS decrease depending on substitution with proline. Asterisks indicate the sites of proline substitutions. Confocal images show representative distribution patterns of the corresponding CAHS proteins (scale bar, 10 μm). Enlarged images are shown as superimposition in each panel (scale bar, 2.5 μm). Blue indicates Hoechst33342 staining of nuclei. The underlying

numerical data are available in S4 Data.
(TIF)

S18 Fig. Representative images of each distribution pattern of proline-substituted CAHS3 and CAHS12 mutants. (A–B) Representative images of granule-like condensation or dispersed distribution of proline-substituted mutants of CAHS3 (A) and CAHS12 (B). Scale bar, 10 μm.
(TIF)

S19 Fig. Distribution patterns of proline-substituted CAHS3 mutants without a GFP-tag in HEp-2 cells under a hyperosmotic condition. (A–B) Distribution patterns of proline-substituted CAHS3 mutants were examined by immunofluorescence for both CAHS3-L207P (A) and CAHS3-L236P (B). Immunostaining images show the dispersed distribution or slightly condensed granules similar to the corresponding CAHS3 mutants labeled with GFP (Fig 3C). Blue indicates DAPI staining of nuclei. Scale bar, 10 μm.
(TIF)

S20 Fig. Significant decrease of the coiled-coil score in the double proline-substituted CAHS3 mutant. Asterisks indicate the proline-substituted mutation sites. The coiled-coil score was calculated from a CAHS3-L207P-L236P amino acid sequence by a prediction tool, COILS. The underlying numerical data are available in S4 Data.
(TIF)

S21 Fig. SDS-PAGE gel images of purified full-length CAHS3 and mutant recombinant proteins. (A–C) Arrowheads indicate major bands corresponding to the expected length of full-length CAHS3 (A), CAHS3-min (B), and CAHS3-L207P proteins (C).
(TIF)

S22 Fig. TFE-dependent reversible gelation of CAHS proteins. (A) Resolubilization of TFE-dependent CAHS3 gelation. CAHS3 gel condensates induced by TFE (final 20%) were redissolved by rinsing with TFE-free PBS. (B) Effect of TFE on BSA solution. TFE (final 20%) had no visible effect on BSA solution (final 4.0 mg/mL). (C and D) TFE-dependent reversible gelation of CAHS8 and CAHS12 proteins. Addition of TFE (final 20%) caused transient gel-transition of CAHS8 (C) and CAHS12 (D) protein solutions (4.0 mg/mL). These gels spontaneously liquefied within several minutes (shown in white letters) after exposure to air. Scale bar, 2 mm.
(TIF)

S23 Fig. Effects of salt and molecular crowding agent on CAHS gelation. (A) High concentration of NaCl (2 M) caused CAHS3 gelation. The CAHS3 gels induced by NaCl did not liquefy exposed to air for 10 min. (B) Addition of the molecular crowding agent, polyethylene glycol (PEG, final 20%) induced turbidity, but no gelation.
(TIF)

S24 Fig. Estimation of the amount of CAHS3 protein in tardigrades. (A) Endogenous CAHS3 protein in *R. varieornatus* lysate was detected by immunoblotting using anti-CAHS3 antibody. Each lane of the lysate (#1 and #2) contains protein amount corresponding to 2 individuals. Diluted series of recombinant CAHS3 proteins were simultaneously analyzed on the same blot as quantification standards. Due to additional His_6-tag, recombinant CAHS3 proteins exhibited slightly higher molecular weight than endogenous ones. Signal intensities were quantified using Fiji imaging software. (B) Based on the immunoblot signal intensity of the diluted series of His_6-CAHS3 protein, the standard curve was generated by a linear regression ($R^2 = 0.9962$). The amount of endogenous CAHS3 protein was estimated as about 3.81 ng per

tardigrade. The underlying numerical data are available in S4 Data (B).
(TIF)

S25 Fig. Predicted 3D structures of a homo-dimer of CAHS3-min proteins by AlphaFold2. (A) pLDDT scores on the prediction corresponding to a tandem CAHS-min amino acid sequence. Scores corresponding to CR1+CR2 regions (70~90) indicated high structure confidence. (B) Two chains of CAHS3-min proteins distinguished by 2 colors. White box indicates the antiparallel helical region. (C) Magnified view of the charge distributions in the juxtaposed helical regions. Green circles indicate the facing of opposite charges between 2 CAHS3-min proteins, suggesting stabilization by electrostatic interactions. (D) Magnified view of the hydrophobicity distributions. Green circles indicate the juxtaposition of similar hydrophobicities/hydrophilicities between 2 proteins, supporting hydrophobic interactions. The underlying numerical data are available in S4 Data (A).
(TIF)

S1 Table. Fluorescent-tagged markers for various cytoskeletons and organelles used in this study.
(PDF)

S1 Movie. A 3D image of CAHS3 filaments in a S2 cell. Cytoskeleton-like distribution of CAHS3-GFP protein in *Drosophila* S2 cell under hyperosmotic cultured medium containing 0.4 M trehalose. Green indicates CAHS3-GFP and blue indicate Hoechst33342 staining of nuclei.
(MP4)

S2 Movie. Movie of filament formation of CAHS3-GFP in HEp-2 cells. Time after medium change to a hyperosmotic condition is shown. CAHS3-GFP simultaneously began to condense at many sites (155 s) and then elongated into filaments (235 s). Scale bar, 5 μm.
(MP4)

S3 Movie. Movie of CAHS3-GFP filament deformation in HEp-2 cells. Time after hyperosmotic medium was replaced with isosmotic medium is shown. CAHS3-GFP filaments simultaneously collapsed and dispersed (400 s). Scale bar, 5 μm.
(MP4)

S1 Data. List of identified 336 T-DRYPs from *Ramazzottius varieornatus*. Each column indicate as follows: (A) Protein ID (*Ramazzottius varieornatus*). (B) Score, Mascot score. (C) Coverage, the coverage by the detected peptides in total residues. (D) # Proteins, the number of the matched proteins. (E) # Unique peptides, the number of the uniquely matched peptides. (F) # Peptides, the number of matched peptides. (G) # PSMs, the number of peptide spectrum matches. (H) #AAs, the number of amino acids. (I) MW [kDa], molecular weight. (J) pI, isoelectric point. (K) IUPred2A, the averaged unstructured scores by IUPred2A. (L) classification, putative taxonomic origins. (M) Human ortholog, orthologous genes of *Homo sapiens*. (N) Fly ortholog, orthologous genes of *Drosophila melanogaster*. (O) Hypsibius exemplaris ortholog (nHd3.0), orthologous genes of *Hypsibius exemplaris*. (S) Paramacrobiotus metropolitanus ortholog, orthologous genes of *Paramacrobiotus metropolitanus* (formerly *Paramacrobiotus* sp. TYO). (P and T)log2FC, log2 fold changes upon desiccation in *H. exemplaris* or *P. metropolitanus*. (Q and U) FDR, false discovery rate in differentially expression analyses between the hydrated and dehydrated states. (R and V) desiccation-change, the classification based on gene regulation upon desiccation. Blank indicates insignificant change (FDR $>$ 0.01), UP indicates log2FC is positive and DOWN indicates log2FC is negative.
(XLSX)

S2 Data. Enrichment analyses of tardigrade tolerance proteins in T-DRYPs.
(XLSX)

S3 Data. List of CAHS protein sequence of 3 tardigrades. Hd, *H. exemplaris* (formerly *H. dujardini*); Pr, *P. metropolitanus* (formerly *Paramacrobiotus* sp. TYO); Rv, *R. varieornatus*.
(XLSX)

S4 Data. Data underlying figures.
(XLSX)

S1 Raw Images. Raw images for Figs 1B, S1, S17 and S20.
(PDF)

Acknowledgments

We are grateful to Tetsuro Hirose for providing the plasmid for FUS-Venus expression and Tokiko Saigo for experimental assistance. Computations were partially performed on the NIG supercomputer at ROIS National Institute of Genetics.

Author Contributions

Conceptualization: Akihiro Tanaka, Tomomi Nakano, Takekazu Kunieda.

Data curation: Akihiro Tanaka, Tomomi Nakano, Gen Honda, Takekazu Kunieda.

Formal analysis: Akihiro Tanaka, Kazutoshi Masuda, Gen Honda, Hiroko Kozuka-Hata, Masaaki Oyama, Miho Yanagisawa, Takekazu Kunieda.

Funding acquisition: Akihiro Tanaka, Takekazu Kunieda.

Investigation: Akihiro Tanaka, Tomomi Nakano, Kento Watanabe, Kazutoshi Masuda, Gen Honda, Shuichi Kamata, Hiroko Kozuka-Hata, Chiho Watanabe.

Methodology: Akihiro Tanaka, Tomomi Nakano, Kento Watanabe, Kazutoshi Masuda, Gen Honda, Hiroko Kozuka-Hata, Takumi Chinen, Daiju Kitagawa, Satoshi Sawai, Masaaki Oyama, Miho Yanagisawa.

Project administration: Takekazu Kunieda.

Resources: Takumi Chinen, Daiju Kitagawa, Satoshi Sawai, Miho Yanagisawa.

Supervision: Takumi Chinen, Daiju Kitagawa, Masaaki Oyama, Miho Yanagisawa, Takekazu Kunieda.

Validation: Akihiro Tanaka, Reitaro Yasui.

Visualization: Akihiro Tanaka, Takekazu Kunieda.

Writing – original draft: Akihiro Tanaka, Takekazu Kunieda.

Writing – review & editing: Akihiro Tanaka, Tomomi Nakano, Kento Watanabe, Kazutoshi Masuda, Shuichi Kamata, Reitaro Yasui, Hiroko Kozuka-Hata, Chiho Watanabe, Takumi Chinen, Daiju Kitagawa, Masaaki Oyama, Miho Yanagisawa, Takekazu Kunieda.

References

1. Keilin D. The problem of anabiosis or latent life: history and current concept. Proc R Soc London Ser B, Biol Sci. 1959; 150:149–191. https://doi.org/10.1098/rspb.1959.0013 PMID: 13633975

2. Møbjerg N, Halberg KA, Jørgensen A, Persson D, Bjørn M, Ramløv H, et al. Survival in extreme environments–on the current knowledge of adaptations in tardigrades. Acta Physiol (Oxf). 2011; 202:409–420. https://doi.org/10.1111/j.1748-1716.2011.02252.x PMID: 21251237

3. Jönsson KI, Rabbow E, Schill RO, Harms-Ringdahl M, Rettberg P. Tardigrades survive exposure to space in low Earth orbit. Curr Biol. 2008; 18:729–731. https://doi.org/10.1016/j.cub.2008.06.048 PMID: 18786368

4. Persson D, Halberg KA, Jørgensen A, Ricci C, Møbjerg N, Kristensen RM. Extreme stress tolerance in tardigrades: Surviving space conditions in low earth orbit. J Zoolog Syst Evol Res. 2011; 49:90–97. https://doi.org/10.1111/j.1439-0469.2010.00605.x

5. Sakurai M, Furuki T, Akao KI, Tanaka D, Nakahara Y, Kikawada T, et al. Vitrification is essential for anhydrobiosis in an African chironomid, Polypedilum vanderplanki. Proc Natl Acad Sci U S A. 2008; 105:5093–5098. https://doi.org/10.1073/pnas.0706197105 PMID: 18362351

6. Clegg JS. The origin of threhalose and its significance during the formation of encysted dormant embryos of Artmia salina. Comp Biochem Physiol. 1965; 14:135–143. https://doi.org/10.1016/0010-406X(65)90014-9

7. Madin KAC, Crowe JH. Anhydrobiosis in nematodes: Carbohydrate and lipid metabolism during dehydration. Exp Zool. 1975; 193:335–342.

8. Erkut C, Penkov S, Khesbak H, Vorkel D, Verbavatz JM, Fahmy K, et al. Trehalose renders the dauer larva of caenorhabditis elegans resistant to extreme desiccation. Curr Biol. 2011; 21:1331–1336. https://doi.org/10.1016/j.cub.2011.06.064 PMID: 21782434

9. Jain NK, Roy I. Effect of trehalose on protein structure. Protein Sci. 2009; 18:24–36. https://doi.org/10.1002/pro.3 PMID: 19177348

10. Hengherr S, Heyer AG, Köhler HR, Schill RO. Trehalose and anhydrobiosis in tardigrades–Evidence for divergence in responses to dehydration. FEBS J. 2008; 275:281–288. https://doi.org/10.1111/j.1742-4658.2007.06198.x PMID: 18070104

11. Hara Y, Shibahara R, Kondo K, Abe W, Kunieda T. Parallel evolution of trehalose production machinery in anhydrobiotic animals via recurrent gene loss and horizontal transfer. Open Biol. 2021; 11:200413. https://doi.org/10.1098/rsob.200413 PMID: 34255978

12. Hand SC, Menze MA, Toner M, Boswell L, Moore D. LEA proteins during water stress: Not just for plants anymore. Annu Rev Physiol. 2011; 73:115–134. https://doi.org/10.1146/annurev-physiol-012110-142203 PMID: 21034219

13. Goyal K, Walton LJ, Tunnacliffe A. LEA proteins prevent protein aggregation due to water stress. Biochem J. 2005; 388:151–157. https://doi.org/10.1042/BJ20041931 PMID: 15631617

14. Belott C, Janis B, Menze MA. Liquid-liquid phase separation promotes animal desiccation tolerance. Proc Natl Acad Sci U S A. 2020; 117:27676–27684. https://doi.org/10.1073/pnas.2014463117 PMID: 33077592

15. Yamaguchi A, Tanaka S, Yamaguchi S, Kuwahara H, Takamura C, Imajoh-Ohmi S, et al. Two novel heat-soluble protein families abundantly expressed in an anhydrobiotic tardigrade. PLoS ONE. 2012; 7: e44209. https://doi.org/10.1371/journal.pone.0044209 PMID: 22937162

16. Hashimoto T, Horikawa DD, Saito Y, Kuwahara H, Kozuka-Hata H, Shin-I T, et al. Extremotolerant tardigrade genome and improved radiotolerance of human cultured cells by tardigrade-unique protein. Nat Commun. 2016; 7:12808. https://doi.org/10.1038/ncomms12808 PMID: 27649274

17. Yoshida Y, Koutsovoulos G, Laetsch DR, Stevens L, Kumar S, Horikawa DD, et al. Comparative genomics of the tardigrades Hypsibius dujardini and Ramazzottius varieornatus. PLoS Biol. 2017; 15: e2002266. https://doi.org/10.1371/journal.pbio.2002266 PMID: 28749982

18. Boothby TC, Tapia H, Brozena AH, Piszkiewicz S, Smith AE, Giovannini I, et al. Tardigrades use intrinsically disordered proteins to survive desiccation. Mol Cell. 2017; 65:975–984. https://doi.org/10.1016/j.molcel.2017.02.018 PMID: 28306513

19. Kamilari M, Jørgensen A, Schiøtt M, Møbjerg N. Comparative transcriptomics suggest unique molecular adaptations within tardigrade lineages. BMC Genomics. 2019; 20:607. https://doi.org/10.1186/s12864-019-5912-x PMID: 31340759

20. Murai Y, Yagi-Utsumi M, Fujiwara M, Tanaka S, Tomita M, Kato K, et al. Multiomics study of a heterotardigrade, Echinisicus testudo, suggests convergent evolution of anhydrobiosis-related proteins in Tardigrada. BMC Genomics. 2021; 22:813. https://doi.org/Doi.org/10.1186/s12864-021-08131-x

21. Arakawa K, Numata K. Reconsidering the "glass transition" hypothesis of intrinsically unstructured CAHS proteins in desiccation tolerance of tardigrades. Mol Cell. 2021; 81:409–410. https://doi.org/10.1016/j.molcel.2020.12.007 PMID: 33545053

22. Fletcher DA, Mullins RD. Cell mechanics and the cytoskeleton. Nature. 2010; 463:485–492. https://doi.org/10.1038/nature08908 PMID: 20110992

23. Pegoraro AF, Janmey P, Weitz DA. Mechanical properties of the cytoskeleton and cells. Cold Spring Harb Perspect Biol. 2017; 9:a022038. https://doi.org/10.1101/cshperspect.a022038 PMID: 29092896

24. Hering L, Bouameur JE, Reichelt J, Magin TM, Mayer G. Novel origin of lamin-derived cytoplasmic intermediate filaments in tardigrades. Elife. 2016; 5:e11117. https://doi.org/10.7554/eLife.11117 PMID: 26840051

25. Goldman RD, Khuon S, Chou YH, Opal P, Steinert PM. The function of intermediate filaments in cell shape and cytoskeletal integrity. J Cell Biol. 1996; 134:971–983. https://doi.org/10.1083/jcb.134.4.971 PMID: 8769421

26. Peter A, Stick R. Evolutionary aspects in intermediate filament proteins. Curr Opin Cell Biol. 2015; 32:48–55. https://doi.org/10.1016/j.ceb.2014.12.009 PMID: 25576801

27. Roccatano D, Colombo G, Fioroni M, Mark AE. Mechanism by which 2,2,2-trifluoroethanol/water mixtures stabilize secondary-structure formation in peptides: a molecular dynamics study. Proc Natl Acad Sci U S A. 2002; 99:12179–12184. https://doi.org/10.1073/pnas.182199699 PMID: 12196631

28. Kentsis A, Sosnick TR. Trifluoroethanol promotes helix formation by destabilizing backbone exposure: desolvation rather than native hydrogen bonding defines the kinetic pathway of dimeric coiled coil folding. Biochemistry. 1998; 37:14613–14622. https://doi.org/10.1021/bi981641y PMID: 9772190

29. Tolleter D, Jaquinod M, Teyssier E, Payet N. Structure and function of a mitochondrial late embryogenesis abundant protein are revealed by desiccation. 2007; 19:1580–1589. https://doi.org/10.1105/tpc.107.050104 PMID: 17526751

30. Koubaa S, Bremer A, Hincha DK, Brini F. Structural properties and enzyme stabilization function of the intrinsically disordered LEA_4 protein TdLEA3 from wheat. Sci Rep. 2019; 9:3720. https://doi.org/10.1038/s41598-019-39823-w PMID: 30842512

31. Sugiura K, Matsumoto M, Kunieda T. Description of a model tardigrade Paramacrobiotus metropolitanus sp. Nov. (Eutardigrada) from Japan with a summary of its life history, reproduction and genomics. Zootaxa. 2022; 5134:92–112. https://doi.org/Doi.org/10.11646/ZOOTAXA.5134.1.4

32. Guo M, Pegoraro AF, Mao A, Zhou EH, Arany PR, Han Y, et al. Cell volume change through water efflux impacts cell stiffness and stem cell fate. Proc Natl Acad Sci U S A. 2017; 114:E8618–E8627. https://doi.org/10.1073/pnas.1705179114 PMID: 28973866

33. Kato M, Han TW, Xie S, Shi K, Du X, Wu LC, et al. Cell-free formation of RNA granules: Low complexity sequence domains form dynamic fibers within hydrogels. Cell. 2012; 149:753–767. https://doi.org/10.1016/j.cell.2012.04.017 PMID: 22579281

34. Herrmann H, Aebi U. Intermediate filaments: structure and assembly. Cold Spring Harb Lab Press. 2016; 8:a018242. https://doi.org/10.1101/cshperspect.a018242 PMID: 27803112

35. Chou PY, Fasman GD. Prediction of protein conformation. Biochemistry. 1974; 13:222–245. https://doi.org/10.1021/bi00699a002 PMID: 4358940

36. Horikawa DD, Kunieda T, Abe W, Watanabe M, Nakahara Y, Yukuhiro F, et al. Establishment of a rearing system of the extremotolerant tardigrade Ramazzottius varieornatus: A new model animal for astrobiology. Astrobiology. 2008; 8:549–556. https://doi.org/10.1089/ast.2007.0139 PMID: 18554084

37. Yagi-Utsumi M, Aoki K, Watanabe H, Song C, Nishimura S, Satoh T, et al. Desiccation-induced fibrous condensation of CAHS protein from an anhydrobiotic tardigrade. Sci Rep. 2021; 11:21328. https://doi.org/10.1038/s41598-021-00724-6 PMID: 34737320

38. Malki AA, Teulon J, Zarco AC, Chen W, Adamski W, Maurin D, et al. Intrinsically Disordered Tardigrade Proteins Self-Assemble into Fibrous Gels in Response to Environmental Stress. Angew Chem Int Ed Engl. 2022; 61:e202109961. https://doi.org/10.1002/anie.202109961 PMID: 34750927

39. Harmon TS, Holehouse AS, Rosen MK, Pappu RV. Intrinsically disordered linkers determine the interplay between phase separation and gelation in multivalent proteins. Elife. 2017; 6:e30294. https://doi.org/10.7554/eLife.30294 PMID: 29091028

40. Jumper J, Evans R, Pritzel A, Green T, Figurnov M, Ronneberger O, et al. Highly accurate protein structure prediction with AlphaFold. Nature. 2021; 596:583–589. https://doi.org/10.1038/s41586-021-03819-2 PMID: 34265844

41. Mirdita M, Schütze K, Moriwaki Y, Heo L, Ovchinnikov S, Steinegger M. ColabFold: making protein folding accessible to all. Nat Methods. 2022. https://doi.org/10.1038/s41592-022-01488-1 PMID: 35637307

42. Protter DSW, Parker R. Principles and properties of stress granules. Trends Cell Biol. 2016; 26:668–679. https://doi.org/10.1016/j.tcb.2016.05.004 PMID: 27289443

43. Franzmann TM, Alberti S. Protein phase separation as a stress survival strategy. Cold Spring Harb Perspect Med. 2019; 9:a034058. https://doi.org/10.1101/cshperspect.a034058 PMID: 30617047

44. LeBlanc BM, Hand SC. Target enzymes are stabilized by AfrLEA6 and a gain of α-helix coincides with protection by a group 3 LEA protein during incremental drying. Biochim Biophys Acta–Proteins. Proteomics. 2021; 1869:140642. https://doi.org/10.1016/j.bbapap.2021.140642 PMID: 33647452

45. Shiraki K, Nishikawa K, Goto Y. Trifluoroethanol-induced stabilization of the alpha-helical structure of beta-lactoglobulin: implication for non-hierarchical protein folding. J Mol Biol. 1995; 245:180–194. https://doi.org/10.1006/jmbi.1994.0015 PMID: 7799434

46. Vincenzi M, Mercurio FA, Leone M. About TFE: Old and new findings. Curr Protein Pept Sci. 2019; 20:425–451. https://doi.org/10.2174/1389203720666190214152439 PMID: 30767740

47. Tsuboyama K, Osaki T, Matsuura-Suzuki E, Kozuka-Hata H, Okada Y, Oyama M, et al. A widespread family of heat-resistant obscure (Hero) proteins protect against protein instability and aggregation. PLoS Biol. 2020; 18:e3000632. https://doi.org/10.1371/journal.pbio.3000632 PMID: 32163402

48. Mészáros B, Erdös G, Dosztányi Z. IUPred2A: Context-dependent prediction of protein disorder as a function of redox state and protein binding. Nucleic Acids Res. 2018; 46:W329–37. https://doi.org/10.1093/nar/gky384 PMID: 29860432

49. Bailey T, Elkan C. Fitting a mixture model by expectation maximization to discover motifs in biopolymers. Proc Int Conf Intell Syst Mol Biol. 1994; 2:28–36. PMID: 7584402

50. Drozdetskiy A, Cole C, Procter J, Barton GJ. JPred4: A protein secondary structure prediction server. Nucleic Acids Res. 2015; 43:W389–W394. https://doi.org/10.1093/nar/gkv332 PMID: 25883141

51. Lupas A, Van Dyke M, Stock J. Predicting coiled coils from protein sequences. Science. 1991; 252:1162–1164. https://doi.org/10.1126/science.252.5009.1162 PMID: 2031185

52. Pettersen EF, Goddard TD, Huang CC, Meng EC, Couch GS, Croll TI, et al. UCSF ChimeraX: Structure visualization for researchers, educators, and developers. Protein Sci. 2021; 30:70–82. https://doi.org/10.1002/pro.3943 PMID: 32881101

53. Mi H, Ebert D, Muruganujan A, Mills C, Albou LP, Mushayamaha T, et al. PANTHER version 16: A revised family classification, tree-based classification tool, enhancer regions and extensive API. Nucleic Acids Res. 2021; 49:D394–D403. https://doi.org/10.1093/nar/gkaa1106 PMID: 33290554

54. Zhou Y, Zhou B, Pache L, Chang M, Khodabakhshi AH, Tanaseichuk O, et al. Metascape provides a biologist-oriented resource for the analysis of systems-level datasets. Nat Commun. 2019; 10:1523. https://doi.org/10.1038/s41467-019-09234-6 PMID: 30944313

55. Kim D, Paggi JM, Park C, Bennett C, Salzberg SL. Graph-based genome alignment and genotyping with HISAT2 and HISAT-genotype. Nat Biotechnol. 2019; 37:907–915. https://doi.org/10.1038/s41587-019-0201-4 PMID: 31375807

56. Liao Y, Smyth GK, Shi W. FeatureCounts: An efficient general purpose program for assigning sequence reads to genomic features. Bioinformatics. 2014; 30:923–930. https://doi.org/10.1093/bioinformatics/btt656 PMID: 24227677

57. Love MI, Huber W, Anders S. Moderated estimation of fold change and dispersion for RNA-seq data with DESeq2. Genome Biol. 2014; 15:550. https://doi.org/10.1186/s13059-014-0550-8 PMID: 25516281

58. Bindels DS, Haarbosch L, Van Weeren L, Postma M, Wiese KE, Mastop M, et al. MScarlet: A bright monomeric red fluorescent protein for cellular imaging. Nat Methods. 2016; 14:53–56. https://doi.org/10.1038/nmeth.4074 PMID: 27869816

59. Sama RRK, Ward CL, Kaushansky LJ, Lemay N, Ishigaki S, Urano F, et al. FUS/TLS assembles into stress granules and is a prosurvival factor during hyperosmolar stress. J Cell Physiol. 2013; 228:2222–2231. https://doi.org/10.1002/jcp.24395 PMID: 23625794

60. Tanaka S, Tanaka J, Miwa Y, Horikawa DD, Katayama T, Arakawa K, et al. Novel mitochondria-targeted heat-soluble proteins identified in the anhydrobiotic tardigrade improve osmotic tolerance of human cells. PLoS ONE. 2015; 10:e0118272. https://doi.org/10.1371/journal.pone.0118272 PMID: 25675104

61. Sakai A, Murayama Y, Fujiwara K, Fujisawa T, Sasaki S, Kidoaki S, et al. Increasing elasticity through changes in the secondary structure of gelatin by gelation in a microsized lipid space. ACS Cent Sci. 2018; 4:477–483. https://doi.org/10.1021/acscentsci.7b00625 PMID: 29721530

62. González M, Martín-Ruíz I, Jiménez S, Pirone L, Barrio R, Sutherland JD. Generation of stable Drosophila cell lines using multicistronic vectors. Sci Rep. 2011; 1:75. https://doi.org/10.1038/srep00075 PMID: 22355594

63. Bullard TA, Borg TK, Price RL. The Expression and Role of Protein Kinase C in Neonatal Cardiac Myocyte Attachment, Cell Volume, and Myofibril Formation Is Dependent on the Composition of the Extracellular Matrix. Microsc Microanal. 2005; 11:224–234. https://doi.org/10.1017/S1431927605050476 PMID: 16060975